Cochlear morphology of Indonesian *Homo erectus* from Sangiran

Abstract

Homo erectus s.l. is key for deciphering the origin and subsequent evolution of genus *Homo*. However, the characterization of this species is hindered by the existence of multiple variants in both mainland and insular Asia, as a result of divergent chronogeographical evolutionary trends, genetic isolation, and interbreeding with other human species. Previous research has shown that cochlear morphology embeds taxonomic and phylogenetic information that may help infer the phylogenetic relationships among hominin species. Here we describe the cochlear morphology of two Indonesian *H. erectus* individuals (Sangiran 2 and 4), and compare it with a sample of australopiths, Middle to Late Pleistocene humans, and extant humans by means of linear measurements and both principal components and canonical variates analyses performed on shape ratios. Our results indicate that *H. erectus* displays a mosaic morphology that combines plesiomorphic (australopith-like) features, (such as a chimp-like round cochlear cross section and low cochlear thickness) with derived characters of later humans (a voluminous and long cochlea, possibly related to hearing abilities)—consistent with the more basal position of *H. erectus*. Our results also denote substantial variation between the two studied individuals, particularly in the length and radius of the first turn, as well as cross-sectional shape. Given the small size of the available sample, it is not possible to discern whether such differences merely reflect intraspecific variation among roughly coeval *H. erectus* individuals or whether they might result from greater age differences between them than currently considered. However, our results demonstrate that most characters found in later humans were already present in Indonesian *H. erectus*, with the exception of Neanderthals, which display an autapomorphic condition relative to other *Homo* species.

Keywords: Fossil humans; Inner ear; Cochlea; Morphometrics; Human Evolution; Southeastern Asia.

1. Introduction

1.1. Homo erectus *from Indonesia*

In 1891, a 'pithecoid' calotte and a 'humanoid' femur allowing for a bipedal stance were discovered at the Trinil site in the island of Java. The following description of *Pithecanthropus erectus* by Dubois (1892) represented a drastic paradigm shift in human evolutionary studies, until then centered in Europe. Subsequent surveys in southeastern Asia by von Koenigswald during the late 1930s led to the discovery of several hominin-bearing sites within the Solo River Basin. The Sangiran Dome, found along a tributary of the Solo River, is one of the richest fossil sites, having yielded several dozen hominin specimens, comprising craniodental and postcranial material and including some remarkably complete crania and numerous calvariae[1] (Koenigswald and Weidenreich, 1939; Weidenreich, 1945; Jacob, 1973; Day, 1986). The dome is formed by a partly eroded anticlinal holding Neogene and Quaternary lacustrine and fluviatile deposits, with two hominin-bearing stratigraphic units: the Lower Pleistocene Pucangan (Sangiran) and the Middle Pleistocene Kabuh (Bapang) Formations. Despite considerable efforts, the lower boundary of the Pucangan Formation, where the oldest hominin remains were found, and thus that of the arrival of *H. erectus* at Java, is still contentious, being dated to either ≥1.5 Ma (Larick et al., 2001; Antón and Swisher, 2004; Zhu et al., 2004; Kaifu et al., 2011), ~1.4 Ma (Matsu'ura et al., 2005; 2020), or ~0.9 Ma (Sémah et al., 2000; Hyodo, 2001). While the specimens recovered from the Kabuh Formation clearly belong to *H. erectus* due to their derived human morphology (Kaifu et al., 2005), the taxonomic allocation of the fossils from the Pucangan Formation is still debated (e.g., Weidenreich, 1945; Koenigswald, 1951; Krantz, 1975; Franzen, 1985a,b; Schwartz and Tattersal, 2003; Schwartz, 2016).

[1] Here we preferred to use 'calvaria', rather than 'calvarium', for referring to the bones constituting the neurocranium. While both wordings are viable singular form alternatives, we decided to follow the main definition by White et al. (2012): "The **calvaria** (or **calvarium**) [emphasis in the original] is the cranium without the face.", which presents calvarium as a secondary option. Furthermore, we considered more advisable to rely on the original Latin word 'calvaria' (feminine, plural: calvariae), rather than on the New Latin term 'calvarium' (neuter, plural: calvaria) that derived from the former later in time.

Over the years, taxonomic opinions about Early Pleistocene Javanese hominins have changed due to different interpretations of the considerable morphological variation expressed by the Pucangan specimens and the presence of homoplastic characters in the dentition of Early Pleistocene *Homo* and *Pongo* (Smith et al., 2009, 2018; Zanolli et al., 2019). At present, following Mayr's (1950) lumping influence, almost all Sangiran hominin specimens are customarily referred to *H. erectus* (albeit not without criticism; Schwartz 2016). However, initially they were variously attributed to multiple taxa (such as *Pithecanthropus robustus, Pithecanthropus dubius, H. erectus modjokertensis, Meganthropus paleojavanicus*, or even *Pongo*) and the allocation of many has changed over time or is still pending (Koenigswald and Weidenreich, 1939; Weidenreich, 1945; Koenigswald, 1950; Krantz, 1975, 1994; Tyler, 2003, 2004, 2006). The great variability of *H. erectus* and the taxonomic uncertainties about this species probably stem from the complex evolutionary context posed by the physiography of the Indonesian archipelago. Eustatic sea-level changes during the Plio-Pleistocene likely led to several isolation phases that would have had a major role in shaping the faunal diversity of this region, including *H. erectus* (Djubiantono and Sémah, 1991; Antón, 2003; Schwartz and Tattersall, 2003). This is further complicated by the possible inclusion of nonhominin specimens within the *H. erectus* hypodigm, as suggested by the resurrection by Zanolli et al. (2019) of *Meganthropus palaeojavanicus* as a valid taxon distinct from *H. erectus*.

The heterogeneity of the Sangiran hominin sample is best exemplified by the partial calvaria Sangiran 2 (S2) and the fragmentary cranium Sangiran 4 (S4; Fig. 1a, b). These specimens represent opposite extremes in terms of gracile and robust cranial proportions, respectively (Santa Luca, 1980). The S2 calvaria shows clear similarities with the *H. erectus* holotype (Trinil 2; Schwartz and Tattersall, 2003), both in size (being fairly small) and morphological details (e.g., the shape of the superior, lateral, and posterior profiles, the low bregmatic swelling, and the slight frontal 'keel'), thus warranting a straightforward attribution to *H. erectus* (e.g., Koenigswald and Weidenreich, 1939). Conversely, S4 has always been subject to controversy, being originally designated as the holotype of *Pithecanthropus*

robustus, and subsequently considered by Weidenreich (1945, 1956) to be an intermediate form between a giant hominid species (such as *Gigantopithecus*) and more gracile *H. erectus*. S4 is indeed thick-boned, being also distinctive by the large and medially located mastoid process and a peculiar drainage pattern in the sigmoid sinus (Schwartz, 2016). The retention of some primitive features in the palate (e.g., the precanine diastemata and the slightly anteriorly projecting canines) even led some authors to question its hominin status (Krantz, 1975, 1994; Tyler, 2003, 2004, 2006), although such a claim seems no longer tenable (Durband, 2008).

1.2. Cochlear morphology and human evolution

Given all these persisting uncertainties about Indonesian *H. erectus*, the analysis of inner anatomical structures that might provide additional taxonomic and phylogenetic information is of utmost significance. This is the case of the bony labyrinth of the inner ear, which has been extensively investigated in hominids (Spoor and Zonneveld, 1994; 1998; Rook et al., 2004; Braga et al., 2015; Le Maître et al., 2017; Urciuoli et al., 2021a) and, especially, hominins (Spoor et al., 1994, 2003; Ni et al., 2010; Braga et al., 2013; Osipov et al., 2013; Wu et al., 2014; Quam et al., 2016; Conde-Valverde et al., 2018; Crevecoeur et al., 2016; Ponce de León et al., 2018; Beaudet, 2019; Beaudet et al., 2019; Ward et al., 2020). The bony labyrinth is composed of the semicircular canals and the vestibule, which encase the vestibular system (in charge of perceiving linear and angular accelerations), as well as the cochlea, which houses the hearing organ. Recent studies have demonstrated that semicircular canals are useful for inferring hominin taxonomic affinities (Braga et al., 2013; Wu et al., 2014; Crevecoeur et al., 2016; Conde-Valverde et al., 2018; Beaudet, 2019; Beaudet et al., 2019) and modern human dispersal distances from Africa (Ponce de León et al., 2018), as well as for phylogenetic reconstruction (Urciuoli et al., 2020; 2021b). In contrast, most studies dealing with the cochlea have investigated the relation between its morphology and hearing function (e.g., Manoussaki et al., 2008; Kirk and Gosselin-Ildari, 2009; Braga et al., 2021), although recent analyses have shown that cochlear shape further

embeds phylogenetically informative characters (Braga et al., 2015; Conde-Valverde et al., 2018; 2019; 2020; Beaudet, 2019; Beaudet et al., 2019).

As a result of the larger number of available Neanderthal specimens, their cochlear morphology has been studied in more detail (Spoor et al., 2003; Beals et al. 2016; Conde-Valverde et al., 2019). Previous studies have reported multiple similarities (some interpreted as homologous and others as homoplastic) in cochlear morphology between Neanderthals and modern humans. In particular, both species share a similarly long first turn of the cochlea (Conde-Valverde et al., 2019), a large cochlear volume (Beals et al., 2016), and a thickened cochlear coiling—all of them interpreted as derived relative to early hominins and chimpanzees (Conde-Valverde et al., 2019). In addition, similarities in cochlear volume have been used to infer a comparable hearing range for modern humans and Neanderthals (Beals et al., 2016), while evidence coming from the outer and middle ear has allowed to reconstruct a similar sound power transmission and occupied bandwidth in both taxa (Conde-Valverde et al., 2021). Finally, Conde-Valverde et al. (2019) identified an evolutionary morphocline among Neanderthals, with younger specimens showing some autapomorphic features (e.g., very low number of cochlear turns and extremely short third turn) that are absent from older specimens such as those from Krapina in Croatia (Beals et al., 2016).

Information about cochlear morphology in Middle Pleistocene humans is limited to the data available only for the sample from Sima de los Huesos in Spain (Conde-Valverde et al., 2019), the Aroeira 3 cranium from Portugal (Conde-Valverde et al., 2020), and Hexian 1 from China (Wu et al., 2014). A detailed analysis of cochlear shape in the Iberian hominins showed that they differ from both Neanderthals and modern humans, by possessing an intermediate morphology between *Pan troglodytes* and Late Pleistocene and Holocene humans. In particular, Middle Pleistocene humans from the Iberian Peninsula display a mosaic of some plesiomorphic hominin features (relatively short first cochlear turn, somewhat rounder cross section, narrow coiling thickness, and fairly small volume) coupled

with characters displayed by later humans (long cochlea relative to their body mass, short third turn, and reduced number of turns; Conde-Valverde et al., 2019, 2020).

Cochlear shape remains largely unexplored in several hominin species, such as *H. erectus*. Aside from Spoor's (1993) seminal work, Braga et al. (2015) first provided information about early hominin cochlear morphology when describing the remains of South African australopiths (*Australopithecus* and *Paranthropus*) and Early Pleistocene *Homo*. These authors highlighted the presence of a phylogenetic signal in the cochlear variables analyzed by them, and suggested that *Homo* species are apomorphic relative to earlier hominins in the possession of a longer cochlea relative to their body size when the length is standardized by the number of cochlear turns—possibly an adaptation for increased hearing sensitivity at low frequencies (Braga et al., 2015). South African hominins have also been inspected by means of 3D geometric morphometrics techniques (Beaudet, 2019; Beaudet et al., 2019), which allowed to identify a unique coiling morphology (with a very tight spiralization, unlike that of other australopiths and modern humans) in early *Homo* specimens (especially SK 27) and a few *Paranthropus* individuals. Unfortunately, this feature has not been analyzed in other early *Homo* specimens, and the evolution of hominin cochlear morphology during the Early Pleistocene is unknown to a large extent, except for brief reports on the *H. erectus* s.l. specimens OH 9 from Olduvai, Tanzania (Spoor, 1993; Spoor and Zonneveld, 1994) and Lantian 1 from China (Wu et al., 2014; Wu and Zhang, 2016).

1.3. Aims of this study

To fill in the gap of knowledge on the cochlear shape morphology of Early Pleistocene humans and explore its implications for the evolution of this anatomical structure in the origins and early evolution of genus *Homo*, here we describe and analyze the cochlear morphology of two *H. erectus* individuals from Sangiran (S2 and S4). This work represents the first detailed description of the cochlear morphology for this species. First, we inspect the cochlear morphology of both specimens by means of linear measurements and shape ratios,

and compare it to that of other Plio-Pleistocene hominins and extant humans using different multivariate approaches. Second, we rely on cochlear morphology to evaluate several competing taxonomic attributions proposed for the analyzed specimens as well as to refine previous evolutionary inferences about this structure regarding the genus *Homo*. Finally, we further infer the hearing ranges of the two *H. erectus* individuals and compare them with those of modern humans and other hominins.

2. Materials and methods

2.1. Studied material

The fossil material analyzed in the present study comprises the S2 calvaria (Koenigswald and Weidenreich, 1939) and S4 fragmentary cranium (partial calvaria and maxilla; Weidenreich, 1945; Schwartz and Tattersall, 2000), both attributed to *H. erectus* (e.g., Schwartz and Tattersall, 2000, 2003). Both specimens were collected from an area that ranges from the Grenzbank zone and the upper levels of the Upper Sangiran formation (~1.4 Ma; Larick et al., 2001; or ~0.9 Ma; Matsu'ura et al., 2020) and are currently housed at the Senckenberg Research Institute and Natural History Museum Frankfurt in Germany as part of the Gustav Heinrich Ralph von Koenigswald collection.

2.2. Comparative sample

The comparative sample (*n* = 42; Table 1) is composed of modern humans (*n* = 10), Neanderthals (*n* = 7), Sima de los Huesos humans (*n* = 10), *Australopithecus* spp. (*n*= 10), *Paranthropus* spp. (*n* = 3), South African early *Homo* (*n* = 2), and Middle Pleistocene *Homo* sp. (*n* = 1). The australopith and early *Homo* specimens come from different South African sites (see Supplementary Online Material [SOM] Table S1), which span from ~4.02–3.67 Ma to 2.01 Ma in the case of *Australopithecus* (Pickering and Kramers, 2010; Granger et al., 2015), and date to ~2.19–1.80 Ma regarding *Paranthropus* and early *Homo* (McKee et al., 1995; Gibbon et al., 2014). The comparative sample of Middle and Late Pleistocene hominins includes individuals from the Sima de los Huesos site (0.43 Ma, Spain; Arsuaga et

al., 2014) together with Neanderthals from France and Israel (71–60 ka; Schwarcz et al., 1989; Rink et al., 2001; Rendu et al., 2014; Guérin et al., 2015; Frouin et al., 2017), as well as the Aroeira 3 cranium from Gruta da Aroeira, Portugal, dated to 0.436–0.389 Ma (Daura et al., 2017). Three-dimensional geometric morphometric techniques could not be applied because 3D models are not available for the Sima de los Huesos and Neanderthal specimens, and hence we relied on linear measurements. As a cautionary note, it must be stressed that some individuals from the comparative sample are subadults (StW 329, SK 27, La Ferrassie 8, Cr. 3, Cr. 7, AT-421, AT-1907) and that some previous analyses have identified ontogenetic changes in the relative orientation of the cochlea relative to the middle and outer ear regions (McRackan et al., 2012). However, the bony labyrinth fully ossifies between 17–19 weeks of gestation and reaches its adult size before birth (Scheuer and Black, 2000; Jeffery and Spoor, 2004), while the variables here employed are unrelated to the orientation of other cranial structures. Therefore, the inclusion of juveniles in the comparative sample—as it is often the case in the literature (e.g., Conde-Valverde et al., 2019; Beaudet et al., 2019)—seems warranted.

2.3. Sample preparation

The S2 and S4 partial crania were µCT-scanned at the Steinmann-Institute of Geology, Mineralogy und Palaeontology at the University of Bonn, using a phoenix V|tome|x S240. For S2, a total of 1300 projections were obtained using voltage = 200 kV and current = 200 µA, with magnification = 4.58, resulting in a voxel size of 0.087 mm after reconstruction. A total of 1500 projections were obtained for S4 with voltage = 180 kV and current = 180 µA, and magnification = 4.54, achieving a voxel size of 0.088 mm after reconstruction. Due to their preservation state, only the right bony labyrinth of each individual was used. The µCT scans of the australopith, early *Homo*, and modern human samples were performed at different facilities (see SOM Table S1 for further information), and reconstructed with voxel sizes ranging between 0.0135 and 0.088 mm. The reconstructed slice stacks were segmented in Avizo v. 7.0 (FEI Visualization Sciences Group, Houston) following the

protocol defined by Kirk and Gosselin-Ildari (2009), which considers the variation in bone density throughout the petrosal. The high-density threshold (HT) has been identified at the first cochlear turn between the lumen and the cortical bone by averaging the maximum and minimum gray values (Spoor and Zonneveld, 1995). Similarly, we identified a low-density threshold (LT) at the boundary between the less dense modiolar bone and the cochlear lumen. Finally, we obtained a high-adjusted threshold (HAT) by averaging LT and HT. The volume of each individual was then obtained as the average of the volumes measured with the LT and HAT. Because the cochlear cavity of some of the fossil specimens was partly or completely filled with matrix (S4, MLD 37/38, STS5, STS19, and SK27), the segmentation was carried out using the HAT only, as already performed by Conde-Valverde et al. (2019) in the case of sediment filled cochlear lumen, with additional manual corrections when there was not enough contrast at the boundary between the bone and the sediment. In the case of the Aroeira 3 individual, we used the reconstructed surface provided by Conde-Valverde et al. (2018: SOM File S1). The 3D models of the cochlea were obtained by separating it from the rest of the bony labyrinth in Avizo, using the position of the round window and of the basilar gap (the gap between the primary and secondary osseous spiral laminae) as reference (Kirk and Gosselin-Ildari, 2009). The meshes were then imported into Geomagic Studio v. 2014.3.0 (3D Systems, Rock Hill) to remove possible self-intersections and non-manifold faces, to fill the holes produced by the cutting with a flat surface, and eventually measure cochlear volume. The µCT scans and 3D models of S2 and S4 are stored in the Senckenberg institutional digital repository and are accessible for the scientific community upon request.

2.4. Data collection and statistical analyses

With the exception Neanderthals and Sima de los Huesos individuals, whose measurements were taken from the literature (Conde-Valverde et al., 2019: SOM Table S1), all the included specimens were directly measured in Avizo using the same landmarks, reference planes, and linear measurements defined by Conde-Valverde et al. (2019). For the

present analysis we relied on a subset of the variables described by Conde-Valverde et al. (2019), including: cochlear length (CL, mm), length of the first turn (L1, mm), length of the third turn (L3, mm), radius of the first turn (R1, mm), radius of the third turn (R3, mm), cochlear volume (Vol, mm^3), angle of the third turn (A3), number of turns (NT; defined as the number of the complete turns + A3/360°), width (Sw, mm), height (Sh, mm), and area (ABT, mm^2) of the first turn cross section, and cochlear thickness (CTh, mm). We also computed the turn proportions (%L1, %L2, and %L3) defined as the length of each turn divided by total cochlear length. All the variables were measured on the 3D model generated using the HAT. Conversely, to ensure direct comparisons with previously published results for primates and hominins (Kirk and Gosselin-Ildari, 2009; Braga et al., 2015; Conde-Valverde et al., 2019), cochlear volume was defined as the average between the volumes obtained using the LT and HAT during segmentation. The ABT was measured in ImageJ (Schneider et al., 2012) on an image of the cross-section taken from a view perpendicular to the cross-sectional plane. For each of the aforementioned variables (except A3, which is used to compute NT), we relied on box-and-whisker plots to assess their variability within the various groups defined in the comparative sample, as well as to compare them with individual fossil specimens.

To investigate the proportions of the cross section at the first cochlear turn, we inspected the correlation between Sh and Sw by means of an ordinary least squares (OLS) allometric regression (using decimal logarithms) performed in R Studio v. 1.1.453 for R v. 3.5.0 (R Core Team, 2019), using the 'stats' package. We also relied on a box-and-whisker plot to assess the variation in the Sw/Sh ratio. To test for significant differences among extant groups, we used an analysis of variance (ANOVA) with Bonferroni-corrected Mann-Whitney post hoc pairwise comparisons performed in R. Furthermore, we computed z-scores ($z = [measurement – mean] / SD$) for individual fossil specimens to test whether they significantly differ ($z > |1.96|$) from the a priori defined groups of the reference sample

We converted the metrical variables into dimensionless shape indices (denoted by an asterisk following variable abbreviations) by dividing the former by the geometric mean of all

the variables in each individual (Mosimann, 1970; Jungers et al., 1995). We then performed a principal components analysis (PCA) on ten shape variables (CL*, L1*, L3*, $Vol^{1/3}$*, Sh*, Sw*, R1*, R3*, CTh*, and NT*; SOM Table S2) to inspect patterns of shape variation. The PCA was performed in R using the 'ade4' v. 1.7-16 package (Dray and Dufour, 2007). We also performed a canonical variate analysis (CVA) on the same shape variables included in the PCA, using the 'Morpho' v. 2.6 package (Schlager, 2017) for R, to assess the closest morphometric affinities of individual fossil specimens by classifying them into various groups defined a priori within the comparative sample. We used modern humans, Neanderthals, australopiths (*Australopithecus* + *Paranthropus*), and Sima de los Huesos humans as a priori defined groups, assuming equally distributed prior probabilities. The *H. erectus* S2 and S4, the early *Homo* SK 27 and SK 847, and the Middle Pleistocene Aroeira 3 specimens were projected a posteriori onto the morphospace identified by the CVA to classify them based on the Mahalanobis squared distances between their projected scores and those of group centroids. For these fossil specimens, we computed cross-validated posterior probabilities as well as typicality probabilities (Albrecht, 1992) of group membership; the latter were obtained using the 'typprobClass' fuction of the 'Morpho' package. Posterior and typicality probabilities rely on different assumptions and are used in a complementary manner. The former assumes that the analyzed individuals must belong to one of the a priori defined group and thus add up to 100% for all the groups together. Conversely, the typicality probabilities allow to evaluate the similarity of an individual to each group separately, based on the distribution of the scores in each group. The classification of individual specimens into one of the a priori defined groups relies on the highest probability in both cases, but the typicality probabilities further represent the *p*-value to test the null hypothesis of membership for each group. In other words, the highest posterior probability denotes the highest morphometric affinities, but a significant typicality probability ($p < 0.05$) might still denote that the specimen does not fit with the variation of the group with the highest posterior probability.

2.5. Estimation of hearing capabilities

To assess hearing capabilities in fossil hominins, we relied on the correlation between the log-transformed cochlear volume and both low and high hearing frequency limits for primates as a whole (Kirk and Gosselin-Ildari, 2009). Conde-Valverde et al. (2019) highlighted some discrepancies between the estimates—based on the regression obtained for the aforementioned correlation —and the empirical values reported by audiogram data for extant humans (Heffner, 2004), thus indicating that the estimated values must be interpreted with caution. Particularly, the empirical values obtained from audiograms of modern humans (Heffner, 2004) demonstrate that this correlation is especially accurate in the case of the low frequency limit (LFL), while it overestimates the high frequency limit (HFL; Conde-Valverde et al., 2019). Hence, besides directly employing the regressions published by Kirk and Gosselin-Ildari (2009) to estimate the hearing frequency limits, we also computed an adjusted high frequency limit value (AHFL). This adjustment was made by multiplying the HFL estimates by a scaling factor corresponding to the quotient between the empirical mean value known for extant humans (17.6 kHz; Heffner, 2004) and the mean estimated for extant humans in the present study. Even if modern humans represent the best option available, as they are the closest extant species to the analyzed fossil taxa, caution should be used when interpreting the adjusted estimates, as the scaling factor is being used across taxa. The variation in estimated LFL and AHFL for the groups included in the comparative sample was inspected by means of box-and-whisker plots. Finally, we computed the z-scores for individual fossil specimens to test whether they significantly differ from the variation of AHFL and LFL displayed by the aforementioned groups.

3. Results

3.1. Description

The right bony labyrinths of S2 and S4 are completely preserved, even if the cochlea of S4 is almost completely filled with sediment, and thus allowed us to readily extract the 3D models of the cochlea (Fig. 1). While both specimens resemble each other in some features, such as the low CTh and intermediate NT, they also display some differences, particularly in

the shape of the first turn cross section (slightly elliptical in S2, round in S4) and in its ABT (larger in S4), the volumetric proportions (smaller Vol in S2 despite a similar CL), and the size of the R1 relative to the R3 (larger in S4; Table 1). The cochlea of S2 shows a narrow CTh (Fig. 1a). It is long and moderately coiled (NT = 2.54), with a not very extended L1 as compared with the somewhat longer L3 relative to L1 and CL. The Vol is moderately large and the first turn cross section has a small area, and appears slightly elliptical (Sw/Sh = 0.86; Fig. 2). The R1 is not very long, being slightly more than twice the size of the R3 (R1/R3 = 2.09). In turn, S4 shows an even narrower cochlea (very low CTh; Fig. 1b) than S2. The CL is long and moderately coiled, quite similar to that of S2. Conversely, the Vol is large and the proportion between L1 and L3 is much higher. The cross section at the first turn is much larger than in S2 and almost perfectly round (Sw/Sh = 0.98; Fig. 2) and the R1 is much longer than the R3 (R1/R3 = 2.75).

3.2. Comparisons

When compared with other fossil hominins and extant humans, the cochlear morphology of S2 appears more primitive (australopith-like) than that of S4 (Fig 3; Table 1). Particularly, the CTh of S2 is very narrow, falling outside the ranges of modern human, Sima de los Huesos and Neanderthals, and being even narrower than in most australopiths (Fig. 3h). The small R1 and L1 of S2 do not fit either with the ranges of variation of modern humans and Neanderthals, and rather resemble those of australopiths and Sima de los Huesos (Fig. 3d,f). When the relative length of the turns is considered, S2 falls instead within the range of both modern humans and australopiths (Fig. 4). The relatively small ABT falls within the range of all groups except modern humans (Fig. 3k), being farther than one SD from the mean of Neanderthals and modern humans only (Table 1). The medium-sized Vol is intermediate between the ranges of humans and australopiths, falling in the overlapping zone between them (below the range of modern humans) and within one SD from the means of all groups except modern humans (Fig 3b). Conversely, the cochlea of S2 shows

similarities with modern humans, Neanderthals and Sima de los Huesos humans in the possession of a long CL, which is longer than in most australopiths (Fig. 3c).

The combination of features found in S4 is unlike that of the other analyzed specimens (Figs. 2 and 3; Table 1). The CTh is very narrow, as in S2 and most australopiths. At the same time, S4 shows closer similarities than S2 with modern humans and fossils attributed to the genus *Homo* (Fig. 1). The CL and L1 are long (longer than in australopiths), similar to those of Neanderthals and modern humans (Fig. 3c, d). Notably, the turn proportions of S4 appear more similar to those of Neanderthals and of Sima de los Huesos humans, while modern humans show a lower %L1 and higher %L3 (Fig. 4). The R1 is long as well, only falling within the range of variation of modern humans (Fig. 3f), and the R1/R3 ratio is larger (R1/R3 = 2.75) than in most of the analyzed specimens. The Vol of S4 is very large, and overlaps only with the range of modern humans, falling at less than one SD from the modern human mean (Fig. 3b; Table 1). The ABT is also large and falls at the high end of the modern human and Neanderthal range (Fig. 3k). Altogether, the values displayed by S4 for Vol, L1, ABT, and R1 resemble those of *Homo* and fall well outside the range of australopiths (Fig. 3b; Table 1). Finally, S4 possesses a round cross section of the first turn, more so than in S2 and in any other analyzed specimen (Fig. 2). Due to the large overlap between the different hominin groups analyzed, the remaining variables (L3 and NT) are slightly less informative, yet they rule out close similarities between Indonesian *H. erectus* and Neanderthals (Fig. 3a, e).

Given that S2 and, especially, S4 differ from extant and fossil humans by the rounder first turn cross section, we investigated the correlation between Sh and Sw by means of an allometric regression (Fig. 2a). Data used for computing the regressions are given in SOM Table S2. The results indicate a significant ($p < 0.001$) isometric correlation between the variables (slope = 0.877 ± 0.251 95% CI; intercept = 0.360 ± 0.147 95% CI; Fig. 2a), albeit with some dispersion ($r^2 = 0.62$), with most australopiths falling below and humans above the best-fit line. The two Sangiran specimens both fall below the regression line, like the early *Homo* SK 27 and the Aroeira 3 specimens. Conversely, SK 847 falls slightly above the

386 regression line, like later and extant humans. Differences in the cross-sectional shape of the
387 first turn are even clearer based on the Sw/Sh ratio. The pairwise comparisons for this ratio
388 denote significant differences between australopiths and all other human groups ($p < 0.001$),
389 while the latter do not significantly differ among each other. In addition, SK847 more closely
390 resembles humans, yet it does not significantly differ from any of the groups based on the z-
391 scores, as neither does SK27, falling in the overlap zone between the upper range of
392 humans and australopiths (Table 2). Similarly, Aroeira 3 occupies an intermediate position
393 between these groups, although it significantly differs from Neanderthals (Table 2).
394 Regarding the studied specimens, S2 most closely resembles australopiths (and does not
395 overlap with humans; Table 2), while S4 possesses a much rounder cross section than any
396 other analyzed specimen (Fig. 2b; SOM Table S2) and falls outside the range of any group
397 (Table 2).
398
399 *3.3. Multivariate shape analyses*
400 Principal components analysis The PCA performed on cochlear shape variables shows a
401 considerable amount of overlap between the analyzed hominin groups and only enables a
402 clear discrimination between australopiths and Neanderthals, as well as between modern
403 humans and Sima de los Huesos (Fig. 5). The shape variation captured by the first principal
404 component (PC1, 48.8% of variance) is mainly driven by differences in R1*, L1*, $Vol^{1/3}$*, CL*,
405 and Sw*, toward negative scores, as well as by L3*, with a positive loading (Fig. 5; Table 3).
406 Hence, the huge amount of overlap along this axis does not allow to discern clearly between
407 the groups, with only a few Neanderthals specimens (most negative values)that could be
408 pulled apart from rest of the comparative sample (intermediate and positive values, except
409 for *Paranthropus*). When the two Indonesian *H. erectus* are considered, S4 falls on
410 moderately negative scores for PC1, outside the range of *Australopithecus* and at the lower
411 range of modern humans and *Paranthropus*, due to its larger Vol* and L1*, as well as the
412 larger radius of the first turn, which mainly resemble the condition found in some
413 Neanderthal individuals. Conversely, S2 fits within the range of variation of all the groups

414 defined in the comparative sample along PC1, as it shows a long CL* coupled with
415 moderately large Vol* and R1*, together with a long L3*. Among the fossil comparative
416 sample, early *Homo* SK 847 shows a morphology that is intermediate between those of S2
417 and S4, while neither the other early *Homo* (SK 27) nor the Aroeira 3 specimens display
418 close morphometric affinities with the studied specimens (Fig. 5).
419 The PC2 (16.8% of variance) is driven by differences in few variables—Sh*, CTh* toward
420 positive and NT* toward negative scores (Table 3). Like for PC1, the overlap between the
421 various groups along PC2 is extensive (Fig. 5). Nonetheless, this axis separates most
422 australopith specimens (moderate to very negative scores) from humans (moderate to very
423 positive scores), due to the broader CTh*, more elliptical cochlear cross section (low Sw/Sh;
424 Fig. 2b) and less coiled cochlea (lower NT*) in the latter. Along PC2, S2 falls clearly outside
425 that of humans (both extant and fossil) and shows closest morphometric affinities with
426 australopiths, especially due to their very narrow CTh*. For the same reason, also S4 and
427 SK 27 fall at the lowest end of the human range on somewhat less negative scores than S2.
428 The other early *Homo* specimen, SK 847, together with the Aroeira 3 individual are found on
429 intermediate PC2 scores, more clearly overlapping with fossil and extant humans due to
430 their larger CTh* (particularly in SK 847) and smaller Sw/Sh ratio (Fig. 2b).
431 When PC1 and PC2 are considered simultaneously, the similarities between S2 and
432 australopiths appear even clearer as the former falls well within the range of the latter and
433 outside the variation of *Homo*. Conversely, S4 does not fit well with the variability of either
434 *Homo* and australopiths, falling outside their convex hulls, albeit very close to Sima de los
435 Huesos and, to a slightly lesser extent, both Neanderthals and australopiths. Similarly,
436 despite some closer affinities with later occurring humans, Aroeira 3 falls outside the convex
437 hulls of modern humans, Sima de los Huesos, and Neanderthal variation, and closer to that
438 of australopiths. In turn, the two early *Homo* individuals also fall apart from one another, with
439 SK 27 markedly departing from the range of variation of the analyzed groups and SK 847
440 falling in the overlap zone between Neanderthals and Sima de los Huesos, not far from
441 modern humans.

Canonical variates analysis The CVA performed on the same ten shape variables used in the PCA correctly classified 97.5% of the specimens (82.5% after cross-validation; Table 4). After cross-validation, all modern humans were correctly classified, while Sima de los Huesos humans show the highest number of misclassified individuals (30%), with two individuals classified as Neanderthals (AT-421 and Cr.13) and one as modern human (AT-1907). In the case of Neanderthals, two specimens were classified as Sima de los Huesos humans (La Ferrassie 8 and Kebara 1), resulting in 71% of correctly classified specimens, a result very close to the one obtained for the Sima de los Huesos humans. Similarly, two australopith specimens (84% correct classification) were misclassified as modern humans (MLD 37/38 and StW 573).

The CVA discriminates well among the four a priori defined groups (Fig. 6), with only minimal overlap between Sima de los Huesos humans and Neanderthals, despite the fact that the three out of four groups belong to genus *Homo*. The first canonical variate (CV1, 64% of variance) discriminates Neanderthals and Sima de los Huesos humans from australopiths and modern humans, and is driven mostly by $Vol^{1/3}$* and R1* and, to a lesser extent, Sw*, all toward negative scores. The Sh* is the only variable possessing a moderately positive effect on the CV1 (Table 5). The CV2 (31% of variance) pulls apart modern humans from australopiths and Sima de los Huesos humans, while Neanderthals occupy an intermediate position. The $Vol^{1/3}$* is the main factor positively influencing CV2 scores, followed by Sh*, L3*, and R1* with similar lower loadings. In contrast, Sw* and NT* drive CV2 toward negative scores with a similar loading (Table 5). Hence, in combination, CV1 and CV2 discriminate well modern humans (with negative CV1 and positive CV2 scores) from other groups due to the larger $Vol^{1/3}$*, longer R1*, more elliptical cross section (low Sw/Sh ratio; Fig. 2b), and moderately higher NT* of the former. Australopiths display negative CV1 and CV2 scores due to the high NT*, moderate $Vol^{1/3}$*, long R1* and L3*, and similarly-sized Sw* and Sh*. Both Sima de los Huesos humans and Neanderthals differ from australopiths and modern humans due to a shorter L3* and lower NT*, combined also with a slightly longer CL*, thus displaying positive scores along CV1. At the same time,

Neanderthals differ from Sima de los Huesos humans by the larger $Vol^{1/3}$* and broader CTh*, thus being somewhat closer to modern humans along CV2 (the moderate positive scores are due to the low NT* in Neanderthals), while Sima de los Huesos humans appear similar to the australopiths condition, characterized by a moderately small $Vol^{1/3}$*, narrow CTh*, and fairly round cochlear cross section (hence falling on negative CV2 scores).

Sangiran 2 falls on moderate negative scores for both CV1 and CV2, at the edge of the convex hull of australopiths and close to the *Paranthropus* specimens. This is due to its moderate $Vol^{1/3}$*, coupled with a low CTh*, fairly long L3*, and slightly elliptical cochlear cross section. Sangiran 4 falls outside the variation of the comparative groups, close to the hull of australopiths on negative CV2 and, particularly, CV1 scores (Fig. 6). Indeed, while the $Vol^{1/3}$* and R1* of S4 are larger than in most australopiths, the Sw/Sh ≈ 1 and narrow CTh* are most similar to those of australopiths rather than *Homo* species. Both SK 847 and Aroeira 3 display moderate negative values for both CV1 and CV2, falling outside the variation of the inspected groups—with SK 847 being almost equidistant from modern humans, Sima de los Huesos humans and australopiths—while Aroeira 3 approaches the convex hull of Sima de los Huesos humans. Finally, SK 27 falls within the convex hull of Sima de los Huesos humans, due to the low NT* combined with a small $Vol^{1/3}$*.

The posterior probabilities of group membership (Table 6) classify the Sangiran specimens as australopiths with very high probabilities even after cross-validation (99.5% and 96.3% for S2 and S4, respectively), thereby denoting closer morphometric affinities in cochlear shape with australopiths. However, while the typicality probabilities of group membership (Table 6) further indicate that S2 significantly differs from the three human groups but not australopiths (and thus confirm its overall australopith-like morphology), S4 represents an outlier for all the groups, suggesting that its cochlear shape does not fit well with the variability displayed by any group. Among the fossil comparative sample (Table 6), SK 847 is classified as an australopith with a high posterior probability (95.5%), as further supported by the typicality probabilities, which do not recover it as an outlier for this group. In turn, Aroeira 3 shows closest affinities with Sima de los Huesos and is classified as such

with a high posterior probability (82.8%), while its typicality probabilities reject the null hypothesis of group membership for all the other groups (Table 6). The early *Homo* SK 27 specimen is the only fossil individual classified as a Neanderthal with a high posterior probability (82.8%). However, as for S4, the typicality probabilities demonstrates that it falls outside the range of variation of any group (Table 6).

3.3. Estimates of auditory capabilities

The LFL and HFL estimates obtained for the studied and comparative samples are reported in Figure 7 and Table 7. The estimated hearing range for modern humans ranges from 24.0 Hz to 20.6 kHz. Our HFL estimates (mean = 20.79 kHz) are on average 15.3% higher than the empirical mean derived for modern humans (17.6 kHz; Heffner, 2004), thereby suggesting that the regression might be overestimating HFL and strengthening the view that HFL estimates should be adjusted.

The results show that S2 matches the range of variation of all the investigated hominin groups except that of modern humans (showing lower values for both AHFL and LFL; Fig. 7; Tables 7 and 8). Nonetheless, the AHFL estimate for S2 (19.85 kHz) is compatible with the nominal range for extant humans, and most similar to the condition estimated for the early *Homo* specimen SK 847 (Fig. 7; Table 7). Sangiran 4, on the other hand, is most similar to modern humans, falling into their distribution for the AHFL and LFL (Fig. 7; Table 7), while it only significantly differs from Sima de los Huesos humans (Table 8). Among the analyzed specimens from the comparative fossil sample, Aroeira 3 is the only one that matches the hearing range of modern humans, while both SK 847 and SK 27 significantly differ from the latter (and SK 27 also from Sima de los Huesos humans and Neanderthals; Fig. 7; Table 8).

4. Discussion

4.1. Cochlear morphology in human evolution

Although our analysis is focused on the cochlear morphology of *H. erectus* from Sangiran, the inspection of the modern human sample adds information about the

intraspecific variability of this species. In particular, our results indicate a higher maximum volume than previous analyses, whereas the minimum value is similar (Beals et al., 2016; Conde-Valverde et al., 2019). Given that all studies have relied on the same segmentation protocol, this result is most likely related to individual variation and suggests a higher intraspecific variability than previously reported for modern humans. Furthermore, the inclusion of other extinct hominins in the fossil comparative sample further allows us to provide insight on the evolution of this anatomical structure from a broader perspective—which is essential for correctly inferring the polarity of change and hence adequately interpreting the cochlear morphology of the investigated specimens. Our results first reveal important cochlear characters of australopiths and South African early *Homo* (Table 9) that remained unnoticed due to the approaches used in previous analyses (Braga et al., 2015; Beaudet, 2019; Beaudet et al., 2019), which did not capture differences in cochlear volume, cross section, and thickness. In particular, our results show that australopiths differ from Middle/Late Pleistocene and extant humans by a rounder cochlear cross section (Sw/Sh ratio closer to 1), shorter L1, and smaller Vol. All three characters were previously identified as hominine symplesiomorphies based on the chimpanzee condition (Conde-Valverde et al., 2019), but our analyses reveal that the plesiomorphic condition for these features was still retained in early hominins (australopiths). In contrast, the two analyzed early *Homo* specimens only appear plesiomorphic in the small Vol and short L1, while more closely resembling later humans (especially SK 847) in the possession of an oval cross section. Our results further indicate that both Neanderthals and modern humans are derived in the long R1, although the comparatively shorter R1 of Sima de los Huesos suggests that such a similarity might be homoplastic feature, as in the case of several other cochlear features (Conde-Valverde et al., 2019)—maybe owing to similar architectural constraints imposed by the course of the facial nerve, which is similar in both species (Spoor et al., 2003) and known to influence the expansion of the cochlear coiling within the petrosal in modern humans (Pietsch et al., 2017).

553 Thanks to the inclusion of a broader comparative sample than in previous studies, our
554 results further imply that some other previous inferences must be reconsidered. Conde-
555 Valverde et al. (2019) suggested that the possession of an oval cross section might be
556 homoplastic between Neanderthals and modern humans, given the retention of a
557 plesiomorphic round cross section in the Sima de los Huesos humans (considered to
558 represent an early stage of the Neanderthal lineage; Arsuaga et al., 2014; Meyer et al.,
559 2016). However, an inspection of the australopith morphology indicates instead that the
560 Sima de los Huesos humans (sharing a similar Sw length with the australopiths, yet
561 possessing a longer Sh) should be regarded as possessing an oval morphology, similar to
562 that of later occurring humans, thereby implying that this feature is likely synapomorphic
563 between Neanderthals and modern humans, at least to some extent. Indeed, the similar
564 morphology displayed by the early *Homo* SK 847, coupled with the intermediate condition
565 found in Aroeira 3 and SK 27, further supports that a somewhat oval cross section might
566 have emerged earlier than previously thought along hominin evolution. Similarly, while it has
567 proposed that both Neanderthals and modern humans are derived in the thicker CTh
568 (Conde-Valverde et al., 2018), the comparison with australopiths indicates that Neanderthals
569 should be rather regarded as less derived than modern humans. Finally, and contrary to
570 previous suggestions, our results for L3, %L3, and NT show that these features vary
571 considerably among hominins. Particularly, *Paranthropus* and early *Homo* display very low
572 values for NT (Braga et al., 2015; Beaudet et al., 2019), L3, and %L3, showing closest
573 similarities with Neanderthals, which are considered autapomorphic for these characters
574 (Conde-Valverde et al., 2019). Accordingly, homoplasy might have also played a role in the
575 evolution of these features. Overall, our results confirm that the ancestral condition for the
576 genus *Homo* most likely included a short CL (both relative to body mass and in absolute
577 value) and L1, a small Vol and R1, low CTh, and a round cross section, while similarities
578 between Neanderthals and extant humans might be homoplastic to a large extent.
579
580 *4.2. Evolutionary and paleobiological implications of Sangiran 2 and 4 cochlear morphology*

Our results demonstrate that the two analyzed *H. erectus* specimens, S2 and S4, are quite different from one another, regardless of some similarities in the long CL—a synapomorphy of humans except its earliest representatives—as well as in the narrow CTh and round cochlear cross section—which are hominine plesiomorphic characters retained by australopiths and some early *Homo* individuals. Such dissimilarities between S2 and S4 may have different explanations. It is generally assumed that S2 and S4 are roughly contemporaneous (Watanabe and Kadar, 1985; Brasseur et al., 2015), but given some uncertainties about the chronostratigraphical provenance of S2 and S4 and the collection methods employed by von Koenigswald's local collaborators (e.g., Tyler and Sartono, 2001), the analyzed Sangiran specimens might come from populations more distant in time from one another than previously assumed. Under the latter assumption, the more derived cochlear morphology of S4 would be suggestive of a younger (late Early/Middle Pleistocene) age relative to S2. However, this is at odds with the clear similarities between S2 and the Trinil 2 specimen (Schwartz and Tattersall, 2003; Schwartz, 2016), dated to the Middle Pleistocene (Berghuis et al., 2021).

Irrespective of age uncertainties, it remains to be ascertained whether the differences between S2 and S4 reflect intraspecific variation (as generally assumed) or are indicative of taxonomic differences at the genus and/or species rank—as formerly concluded by previous authors that assigned S4 to a different species (Weidenreich, 1945) or even suggested pongine affinities (Krantz, 1975, 1994; Tyler, 2003, 2004, 2006). The cochlear morphology of S4, together with its palate and dental morphology (Durband, 2008), allow us to rule out the latter claim. Indeed, despite the plesiomorphic cross section of the first turn (falling close to the high end of the chimpanzee distribution; Conde-Valverde et al., 2019), the larger Vol and R1 and longer L1 of S4 suggest closer affinities with Neanderthals and modern humans than in the case of S2. Given the small sample available, the differences between S2 and S4 might simply reflect opposite ends of the intraspecific range of cochlear morphology variation of *H. erectus.* Despite considerable differences in robusticity between S2 and S4 (Santa Luca, 1980), their conspecific status is supported by their similarities in external cranial

609 morphology to the *H. erectus* holotype (Koenigswald, 1940; Schwartz and Tattersal, 2003;
610 Schwartz, 2016), as well as by the overall marked variation within the *H. erectus* hypodigm
611 as currently conceived (Antón, 2003; Rightmire, 1990; Thorne and Wolpoff, 1982; Wolpoff,
612 1996; Wolpoff et al., 2001). Under such an assumption, it may be inferred that Indonesian *H.*
613 *erectus* would have probably displayed, on average, an intermediate cochlear morphology
614 between S2 and S4, and thus more derived than in australopiths and early *Homo*, but less
615 so than in later humans. Unfortunately, the scanty information on the cochlear morphology of
616 other Early and Middle Pleistocene *H. erectus* (Wu et al., 2014; Wu and Zhang, 2016) does
617 not favor either interpretation. Additional inner ear material of *H. erectus* s.l. from both Africa
618 and Asia should be inspected to test between these competing hypotheses in the future.
619 From a paleobiological viewpoint—and irrespective of the taxonomic and evolutionary
620 interpretation of differences in cochlear morphology between S2 and S4—the large Vol
621 found in S4 (and the hearing range estimated from it) closely resembles that of Neanderthals
622 and modern humans. Even if potentially variable, this is suggestive of a lowered high-
623 frequency cutoff, a possible homoplastic character for both taxa (Conde-Valverde et al.,
624 2019). This result is broadly compatible with an increased sensitivity to low frequencies,
625 which is a modern human autapomorphy relative to other primates (Heffner, 2004). Hence,
626 the S4 individual, and perhaps *H. erectus* more generally, currently represents the earliest
627 occurrence of a modern human-like hearing range, although this by itself cannot be used as
628 direct evidence suggestive of advanced speech capabilities.
629 Indeed, *H. erectus* s.l. is the first hominin species to clearly display a suite of human-like
630 adaptations, including not only a modern brain organization despite smaller cranial capacity
631 (Holloway et al., 2009; Ponce de León et al., 2021), but further encompassing a very
632 committed terrestrial bipedalism (Harcourt-Smith, 2015), a more advanced (albeit not
633 completely modern human-like) pattern of dental development and inferred life-history profile
634 (Kelley and Bolter, 2013), and especially a diet including significant amounts of meat (Milton,
635 1999; Ben-Dor et al., 2021) and systematic stone tool-making abilities (Joordens et al.,
636 2015), both associated with the so-called human predatory pattern (Thompson et al., 2019).

All these characteristics suggests that *H. erectus* s.l. represented the emergence of a new hominin adaptive type (Wood and Collard, 1999), not fundamentally different from that further elaborated by later humans. There is strong evidence in favor of the coevolution between behavioral complexity and enhanced vocal communication abilities (Conde-Valverde et al., 2021). Therefore, the possession—as hinted by the estimates obtained here for S4—of a more modern-human-like hearing range in *H. erectus* than in any of its predecessors may be hypothesized and should be subjected to more detailed investigation in the future.

5. Conclusions

Our analyses indicate that cochlear morphology adequately distinguishes australopiths from humans and further discriminates different human groups despite the presence of homoplasies between modern humans and Neanderthals. Australopiths display overall a plesiomorphic condition that confirms the ancestral morphotype previously inferred for hominins—characterized by a short cochlear length (both in absolute and relative terms), small volume, round cross-sectional shape, and short first cochlear turn. In turn, early *Homo* specimens appear slightly more derived toward the modern human condition but less so than later fossil humans. The inclusion of australopiths in the comparative sample allowed us to refine the polarity of some characters, as well as to identify additional derived features for humans. Based on these considerations, the studied specimens of Indonesian *H. erectus* from Sangiran display a mosaic of plesiomorphic (australopith-like) and derived features, consistent with their more basal status than other humans analyzed except for early *Homo*.

Both Sangiran specimens are largely plesiomorphic in cochlear thickness and cross-sectional shape. Nevertheless, they also differ from one another in some other features. Namely, S4 appears more derived toward later humans in its larger volume and longer and larger first cochlear turn, while at the same time it retains an extremely round, chimpanzee-like cross section. It cannot be completely ruled out that such differences result from S2 and S4 belonging to different species and/or populations more distant in time than customarily

assumed. However, based on similarities in cranial morphology—between them and relative to other Indonesian specimens—the most plausible interpretation is that the differences between S2 and S4 just represent opposite ends of the range of variation displayed by *H. erectus* in cochlear morphology. The inspection of additional specimens of *H. erectus* s.l. from both Africa and Asia will hopefully shed further light on this matter in the future, with implications for understanding the entangled evolutionary history of hominins in southeastern Asia and elsewhere.

In the meantime, the remarkable similarities between the hearing range estimated for S4 and those of Neanderthals and modern humans deserve further attention. In agreement with previous inferences for Neanderthals, this suggests that *H. erectus* might have been more modern-human-like than its hominin forerunners (including early *Homo* representatives) in terms of hearing capabilities—consistent with other morphological and behavioral innovations indicating that *H. erectus* s.l. was the first hominin to clearly display a human-like adaptive strategy.

Acknowledgments

This work has been funded by the Agencia Estatal de Investigación (PID2020-117289GB-I00 and PID2020-116908GB-I00, AEI/FEDER, EU) and the Generalitat de Catalunya (CERCA Programme and Consolidated Research Group 2017 SGR SGR 116). We express our gratitude to the Werner Reimers Foundation in Bad Homburg, which provides the Gustav Heinrich Ralph von Koenigswald collection as a permanent loan for scientific research to the Senckenberg Research Institute and Natural History Museum Frankfurt. We would like to thank C. Zanolli for technical and scientific discussion, as well as the following people and institutions for granting access to and/or performing the CT scans of the comparative material: the University of the Witwatersrand, the Ditsong National Museum of Natural History, the Max Plank Institute for Evolutionary Anthropology, Steinmann-Institute of Geology, Mineralogy und Palaeontology at the University Bonn, M. Tawane, J. Braga, J. Kudakwashe Jakata, and G. Chinamatira. The support of the AESOP+ program is hereby

693 acknowledged. We are also thankful to the DST-NRF for allowing access to the Micro-XCT
694 facility at Necsa. We thank the Guest Editors (C. Zanolli, S. Xing, and Y. Zhang) of the
695 special issue “Asian Pleistocene Hominids” for inviting us to contribute.
696

697 **References**

698 Albrecht, G., 1992. Assessing the affinities of fossils using canonical variates and
699 generalized distances. Hum. Evol. 7, 49–69.
700 Antón, S.C., 2003. Natural history of *Homo erectus*. Yearb. Phys. Anthropol. 46, 126–70.
701 Antón, S.C., Swisher, C.C. III, 2004. Early dispersals of *Homo* from Africa. Annu. Rev.
702 Anthropol. 33, 271–296.
703 Armstrong, S.D., Bloch, J.I., Houde, P., Silcox, M.T., 2011. Cochlear labyrinth volume in
704 euarchontoglirans: implications for the evolution of hearing in Primates. Anat. Rec. 294,
705 263–266.
706 Arsuaga, J.L., Martínez, I., Arnold, L., Aranburu, A., Gracia-Téllez, A., Sharp, W., Quam, R.,
707 Falguères, C., Pantoja-Pérez, A., Bischoff, J., Poza-Rey, E., Parés, J., Carretero, J.,
708 Demuro, M., Lorenzo, C., Sala, N., Martinon-Torres, M., García, N., Alcázar de Velasco,
709 A., Cuenca-Bescós, G., Gómez-Olivencia, A., Moreno, D., Pablos, A., Shen, C.,
710 Rodríguez, L., Ortega, A., García, R., Bonmatí, A., Bermúdez de Castro, J.M., Carbonell,
711 E., 2014. Neandertal roots: Cranial and chronological evidence from Sima de los Huesos.
712 Science 344, 1358–1363.
713 Beals, M.E., Frayer, D.W., Radovčić, J., Hill, C.A., 2016. Cochlear labyrinth volume in
714 Krapina Neandertals. J. Hum. Evol. 90, 176–182.
715 Beaudet, A., 2019. The inner ear of the *Paranthropus* specimen DNH 22 from Drimolen,
716 South Africa. Am. J. Phys. Anthropol. 170, 439–446.
717 Beaudet, A., Clarke, R. J., Bruxelles, L., Carlson, K. J., Crompton, R., de Beer, F., Dhaene,
718 J., Heaton, J. L., Jakata, K., Jashashvili, T., Kuman, K., McClymont, J., Pickering, T. R.,
719 Stratford, D., 2019. The bony labyrinth of StW 573 (“Little Foot”): Implications for early
720 hominin evolution and paleobiology. J. Hum. Evol. 127, 67–80.

721 Ben-Dor, M., Sirtoli, R., Barkai, R., 2021. The evolution of the human trophic level during the
722 Pleistocene. Yearb. Phys. Anthropol. 175, 27–56.
723 Berghuis, H.W.K., Veldkamp, A., Adhityatama, S., Hilgen, S.L., Sutisna, I., Barianto, D.H.,
724 Pop, E.A., Reimann, T., Yurnaldi, D., Ekowati, D.R., Vonhof, H.B., van Kolfschoten, T.,
725 Simanjuntak, T., Schoorl, J.M., Joordens, J.C.A., 2021. Hominin homelands of East Java:
726 Revised stratigraphy and landscape reconstructions for Plio-Pleistocene Trinil. Quat. Sci.
727 Rev. 260, 106912.
728 Braga, J., Thackeray, J.F., Dumoncel, J., Descouens, D., Bruxelles, L., Loubes, J.M., Kahn,
729 J.L., Stampanoni, M., Bam, L., Hoffman, J., de Beer, F., 2013. A new partial temporal
730 bone of a juvenile hominin from the site of Kromdraai B (South Africa). J. Hum. Evol. 65,
731 447–456.
732 Braga, J., Loubes, J.-M., Descouens, D., Dumoncel, J., Thackeray, J.F., Kahn, J.-L., de
733 Beer, F., Riberon, A., Hoffman, K., Balaresque, P., Gilissen, E., 2015. Disproportionate
734 cochlear length in genus *Homo* shows a high phylogenetic signal during apes' hearing
735 evolution. PLoS One 10, e0127780.
736 Braga, J., Samir, C., Fradi, A., Feunteun, Y., Jakata, K., Zimmer, V.A., Zipfel, B., Thackeray,
737 J.F., Macé, M., Wood, B.A., Grine, F.E., 2021. Cochlear shape distinguishes southern
738 African early hominin taxa with unique auditory ecologies. Sci. Rep. 11, 17018.
739 Brasseur, B., Sémah, F., Sémah, A.-M., Djubiantono, T., 2015. Pedo-sedimentary dynamics
740 of the Sangiran dome hominid bearing layers (Early to Middle Pleistocene, central Java,
741 Indonesia): A palaeopedological approach for reconstructing '*Pithecanthropus'* (Javanese
742 *Homo erectus*) palaeoenvironment. Quat. Int. 376, 84–100.
743 Conde-Valverde, M., Quam, R., Martínez, I., Arsuaga, J.L., Daura, J., Sanz, M., Zilhão, J.,
744 2018. The bony labyrinth in the Aroeira 3 Middle Pleistocene cranium. J. Hum. Evol. 124,
745 105–116.
746 Conde-Valverde, M., Martínez, I., Quam, R., Bonmatí, A., Lorenzo, C., Velez, A.D.,
747 Martínez-Calvo, C., Arsuaga, J.L., 2019. The cochlea of the Sima de los Huesos

748 hominins (Sierra de Atapuerca, Spain): New insights into cochlear evolution in the genus
749 *Homo* J. Hum. Evol. 136, 102641.
750 Conde-Valverde, M., Martínez, I., Quam, R., Arsuaga, J.L., Daura, J., Sanz, M., Zilhão, J.,
751 2020. The cochlea of the Aroeira 3 Middle Pleistocene cranium—a comparative study. J.
752 Hum. Evol. 148, 102887.
753 Conde-Valverde, M., Martínez, I., Quam, R.M., Rosa, M., Velez, A.D., Lorenzo, C., Jarabo,
754 P., de Castro, J.M.B., Carbonell, E., Arsuaga, J.L., 2021. Neanderthals and *Homo*
755 *sapiens* had similar auditory and speech capacities. Nat. Ecol. Evol. 5, 609–615.
756 Crevecoeur, I., Brooks, A., Ribot, I., Cornelissen, E., Semal, P., 2016. Late Stone Age
757 human remains from Ishango (Democratic Republic of Congo): New insights on Late
758 Pleistocene modern human diversity in Africa. J. Hum. Evol. 96, 35–57.
759 Daura, J., Sanz, M., Arsuaga, J.L., Hoffmann, D.L., Quam, R.M., Ortega, M.C., Santos, E.,
760 Gómez, S., Rubio, A., Villaescusa, L., Souto, P., Mauricio, J., Rodrigues, F., Ferreira, A.,
761 Godinho, P., Trinkaus, E., Zilhão, J., 2017. New Middle Pleistocene hominin cranium from
762 Gruta da Aroeira (Portugal). Proc. Natl. Acad. Sci. USA 114, 3397–3402.
763 Day, M., 1986. Guide to Fossil Man, 4th ed. University of Chicago Press, Chicago.
764 Djubiantono, T., Sémah, F., 1991. Lower Pleistocene marine-continental transitional beds in
765 the Solo depression and their relation to the environment of the Pucangan hominids. Bull.
766 Indo-Pac. Prehist. Assoc. 11, 7–13.
767 Dray, S., Dufour, A., 2007. The ade4 package: Implementing the duality diagram for
768 ecologists. J. Stat. Softw. 22, 1–20.
769 Dubois, E., 1892. Palaeontologische andrezoekingen op Java. Versl. Mijnw. Batavia 3, 10–
770 14.
771 Durband, A.C., 2008. The enigma of the Sangiran 4 palate revisited. HOMO 59, 111–122.
772 Ferring, R., Oms, O., Agustí, J., Berna, F., Nioradze, M., Shelia, T., Tappen, M., Vekua, A.,
773 Zhvania, D., Lordkipanidze, D., 2011. Earliest human occupations at Dmanisi (Georgian
774 Caucasus) dated to 1.85–1.78 Ma. Proc. Natl. Acad. Sci. USA 108, 10432–10436.

775 Franzen, J.L., 1985a. Asian australopithecines? In: Tobias, P.V. (Ed.), Hominid Evolution:
776 Past, Present, and Future. Wiley-Liss, New York, pp. 255–263.
777 Franzen, J.L., 1985b. What is ‘‘*Pithecanthropus dubius* Koenigswald, 1950’’? In: Delson, E.
778 (Ed.), Ancestors: The Hard Evidence. Alan R Liss, New York, pp. 221–226.
779 Frouin, M., Lahaye, C., Valladas, H., Higham, T., Debénath, A., Delagnes, A., Mercier, N.,
780 2017. Dating the middle Paleolithic deposits of La Quina Amont (Charente, France) using
781 luminescence methods. J. Hum. Evol 109, 30–45.
782 Gibbon, R.J., Pickering, T.R., Sutton, M.B., Heaton, J.L., Kuman, K., Clarke, R.J., Brain,
783 C.K., Granger, D.E., 2014. Cosmogenic nuclide burial dating of hominin bearing
784 Pleistocene cave deposits at Swartkrans, South Africa. Quat. Geochronol. 24, 10–15.
785 Granger, D.E., Gibbon, R.J., Kuman, K., Clarke, R.J., Bruxelles, L., Caffee, M.W., 2015.
786 New cosmogenic burial ages for Sterkfontein Member 2 *Australopithecus* and Member 5
787 Oldowan. Nature 522, 85–88.
788 Guérin, G., Frouin, M., Talamo, S., Aldeias, V., Bruxelles, L., Chiotti, L., Dibble, H.L.,
789 Goldberg, P., Hublin, J.-J., Jain, M., 2015. A multi-method luminescence dating of the
790 Palaeolithic sequence of La Ferrassie based on new excavations adjacent to the La
791 Ferrassie 1 and 2 skeletons. J. Archaeol. Sci. 58, 147–166.
792 Harcourt-Smith, W.E.H., 2015. The origins of bipedal locomotion. In: Henke, W., Tattersall, I.
793 (Eds.), Handbook of Paleoanthropology, 2nd ed. Springer Verlag, Heidelberg, pp. 1919–
794 1959.
795 Heffner, R.S., 2004. Primate hearing from a mammalian perspective. Anat. Rec. 281,
796 1111e1122.
797 Holloway R.L., 1981. The indonesian *Homo erectus* brain endocasts revisited. Am. J. Phy.
798 Anthropol. 55, 503–521.
799 Holloway, R.L., Sherwood, C.C., Hof, P.R., Rilling, J.K., 2009. Evolution of the brain in
800 humans – Paleoneurology. In: The New Encyclopedia of Neuroscience: Springer, pp.
801 1326–1334.

Hyodo, M., 2001. The Sangiran geomagnetic excursion and its chronological contribution to the Quaternary geology in Java. In: Simanjuntak, H.T., Prasetyo, B., Handini, R. (Eds.), Sangiran: Man, Culture and Environment in Pleistocene Times. Yayasan Obor Indonesia, Jakarta, pp. 320–335.

Jacob, T., 1973. Paleoanthropological discoveries in Indonesia with special reference to the finds of the last two decades. J. Hum. Evol. 2, 473–485.

Jeffery, N., Spoor, F., 2004. Prenatal growth and development of the modern human labyrinth. J. Anat. 204, 71–92.

Joordens, J.C.A., d'Errico, F., Wesselingh, F.P., Munro, S., de Vos, J., Wallinga, J., Ankjærgaard, C., Reimann, T., Wijbrans, J.R., Kuiper, K.F., Mücher, H.J., Coqueugniot, H., Prié, V., Joosten, I., van Os, B., Schulp, A.S., Panuel, M., van der Haas, V., Lustenhouwer, W., Reijmer, J.J.G., Roebroeks, W., 2015. *Homo erectus* at Trinil on Java used shells for tool production and engraving. Nature 518, 228–231.

Jungers, W.L., Falsetti, A.B., Wall, C.E., 1998. Shape, relative size, and size-adjustments in morphometrics. Yearb. Phys. Anthropol. 38, 137–161.

Kaifu, Y., Zaim, Y., Baba, H., Kurniawan, I., Kubo, D., Rizal, Y., Arif, J., Aziz, F., 2011. New reconstruction and morphological description of a *Homo erectus* cranium Skill IX (Tjg-1993.05) from Sangiran, Central Java. J. Hum. Evol. 61, 270–294.

Kelley, J., Bolter, D., 2013. Growth, development, and life history in hominin evolution. In: Begun, D.R. (Ed.), A Companion to Paleoanthropology. Blackwell Publishing, Chichester, pp. 97–117.

Kirk, E.C., Gosselin-Ildari, A.D., 2009. Cochlear labyrinth volume and hearing abilities in primates. Anat Rec. 292, 765–776.

Koenigswald, G.H.R. von, 1940. Neue *Pithecanthropus*-Funde 1936-1938. Ein Beitrag zur Kenntnis der Praehominiden. Wetenschappelijke Mededeelingen Dienst Mijnbouw in Nederlandsch-Indië 28, 1–232.

Koenigswald, G.H.R. von, 1951. Introduction. In: Weidenreich, F. (Ed.), Morphology of Solo Man. Anthropol. Pap. Am. Mus. Nat. Hist. 43, 205–290.

Koenigswald, G.H.R. von, Weidenreich, F., 1939. The relationships between *Pithecanthropus* and *Sinanthropus*. Nature 144, 926–929.

Krantz, G.S., 1975. An explanation for the diastema of Javan erectus skull IV. In: Tuttle, R.H. (Ed.), Paleoanthropology, Morphology and Paleoecology. Mouton Publishers, The Hague, pp. 361–372.

Krantz, G.S., 1994. The palate of skull Sangiran 4 from Java. Cour. Forsch.-inst. Senck. 171, 69–74.

Larick, R., Ciochon, R.L., Zaim, Y., Sudijono, Suminto, Rizal, Y., Aziz, F., Reagan, M., Heizler, M., 2001. Early Pleistocene $^{40}Ar/^{39}Ar$ ages for Kabuh Formation hominins, Central Java, Indonesia. Proc. Natl. Acad. Sci. USA 98, 4866–4871.

Le Maître, A., Schuetz, P., Vignaud, P., Brunet, M., 2017. New data about semicircular canal morphology and locomotion in modern hominoids. J. Anat. 231, 95–109.

Manoussaki, D., Chadwick, R.S., Ketten, D.R., Arruda, J., Dimitriadis, E.K., O'Malley, J.T., 2008. The influence of cochlear shape on low-frequency hearing. Proc. Natl. Acad. Sci. USA 105, 6162–6166.

Matsu'ura, S., Kondo, M., Takeshita, Y., Kumai, H., Hyodo, M., Kamishima, Y., Kaneda, T., Aziz, F., 2005. Probable source horizon of the *Pithecanthropus* II (Sangiran 2) calotte and its possible palaeoanthropological implications. Anthropol. Sci. 113, 323.

Matsu'ura, S., Kondo, M., Danhara, T., Sakata, S., Iwano, H., Hirata, T., Kurniawan, I., Setiyabudi, E., Takeshita, Y., Hyodo, M., Kitaba, I., Sudo, M., Danhara, Y., Aziz, F., 2020. Age control of the first appearance datum for Javanese *Homo erectus* in the Sangiran area. Science 367, 210–214.

Mayr, E., 1950. Taxonomic categories in fossil hominids. Cold Spr. Harb. Symp. Quant. Biol. 15,109–118.

McKee, J.K., Thackeray, J.F., Berger, L.R., 1995. Faunal assemblage seriation of Southern African Pliocene and Pleistocene fossil deposits. Am. J. Phys. Anthropol. 96, 235–250.

McRackan, T.R., Reda, F.A., Rivas, A., Noble, J.H., Deitrich, M.M., Dawant, B.M., Labadie, R.F., 2012. Comparison of cochlear implant relevant anatomy in children versus adults. Otol. Neurotol. 33, 328–334.

Meyer, M., Arsuaga, J.L., de Filippo, C., Nagel, S., Aximu-Petri, A., Nickel, B., Martínez, I., Gracia, A., Bermúdez de Castro, J.M., Carbonell, E., Viola, B., Kelso, J., Prüfer, K., Pääbo, S., 2016. Nuclear DNA sequences from the Middle Pleistocene Sima de los Huesos hominins. Nature 531, 504–507.

Milton, K., 1999. A hypothesis to explain the role of meat-eating in human evolution. Evol. Anthropol. 8, 11–21.

Mosimann, J.E., 1970. Size allometry: Size and shape variables with characterizations of the log-normal and gamma distributions. J. Am. Stat. Assoc. 56, 930–-945.

Ni, X., Flynn, J.J., Wyss, A. R., 2010. The bony labyrinth of the early platyrrhine primate *Chilecebus*. J. Hum. Evol. 59, 595–607.

Osipov, B., Harvati, K., Nathena, D., Spanakis, K., Karantanas, A., Kranioti, E. F., 2013. Sexual dimorphism of the bony labyrinth: A new age-independent method. Am. J. Phys. Anthropol. 151, 290–301.

Pickering, R., Kramers, J.D., 2010. Reappraisal of the stratigraphy and determination of new U-Pb dates for the Sterkfontein hominid site, South Africa. J. Hum. Evol. 59, 70–86.

Pietsch, M., Davila, L.A., Erfurt, P., Avci, E., Lenarz, T., Kral, A., 2017. Spiral form of the human cochlea results from spatial constraints. Sci. Rep. 7, 7500.

Ponce de León, M.S., Koesbardiati, T., Weissmann, J.D., Milella, M., Reyna-Blanco, C.S., Suwa, G., Kondo, O., Malaspinas, A.-S., White, T.D., Zollikofer, C.P.E., 2018. Human bony labyrinth is an indicator of population history and dispersal from Africa. Proc. Natl. Acad. Sci. USA 115, 4128–4133.

Ponce de León, M.S., Bienvenu, T., Marom, A., Engel, S., Tafforeau, P., Warren, J.L.A., Lordkipanidze, D., Kurniawan, I., Murti, D.B., Suriyanto, R.A. Koesbardiati, T., Zollikofer, C.P.E., 2021. The primitive brain of early *Homo*. Science 372, 165–171.

Quam, R.M., Martínez, I., Rosa, M., Bonmatí, A., Lorenzo, C., de Ruiter, D.J., Moggi-Cecchi, J., Conde-Valverde, M., Jarabo, P., Menter, C.G., Thackeray, J.F., Arsuaga, J.L., 2015. Early hominin auditory capacities. Sci. Adv. 1, e1500355.

Quam, R., Lorenzo, C., Martínez, I., Gracie-Téllez, A., Arsuaga, J.L., 2016. The bony labyrinth of the middle Pleistocene Sima de los Huesos hominins (Sierra de Atapuerca, Spain). J. Hum. Evol. 90, 1–15.

R Core Team, 2019. R: A language and environment for statistical computing. R Foundation for Statistical Computing, Vienna.

Rendu, W., Beauval, C., Crevecoeur, I., Bayle, P., Balzeau, A., Bismuth, T., Bourguignon, L., Delfour, G., Faivre, J.-P., Lacrampe-Cuyaubère, F., 2014. Evidence supporting an intentional Neandertal burial at La Chapelle-aux-Saints. Proc. Natl. Acad. Sci. USA 111, 81–86.

Rightmire, P., 1990. The Evolution of *Homo erectus*. Cambridge University Press, Cambridge.

Rink, W., Schwarcz, H., Lee, H., Rees-Jones, J., Rabinovich, R., Hovers, E., 2001. Electron spin resonance (ESR) and thermal ionization mass spectrometric (TIMS) $^{230}Th/^{234}U$ dating of teeth in Middle Paleolithic layers at Amud Cave, Israel. Geoarchaeology 16, 701–717.

Rook, L., Bondioli, L., Casali, F., Rossi, M., Köhler, M., Moyá-Solá, S., Macchiarelli, R., 2004. The bony labyrinth of *Oreopithecus bambolii*. J. Hum. Evol. 46, 349–356.

Santa Luca, A.P., 1980. The Ngandong Fossil Hominids: A Comparative Study of a Far Eastern *Homo erectus* Group. Yale University Press, New Haven.

Scheuer, L., Black, S., 2000. Developmental Juvenile Osteology. Academic Press, San Diego.

Schlager, S., 2017. Morpho and Rvcg-shape analysis in R: R-packages for geometric morphometrics, shape analysis and surface manipulations. In: Zheng, G., Li, S., Székely, G. (Eds.), Statistical Shape and Deformation Analysis. Methods, Implementation and Applications. Academic Press, London, pp. 217–256.

910 Schneider, C.A., Rasband, W.S., Eliceiri, K.W., 2012. NIH Image to ImageJ: 25 years of
911 image analysis. Nat. Methods 9, 671–675.
912 Schwarcz, H., Buhay, W., Grün, R., Valladas, H., Tchernov, E., Bar-Yosef, O.,
913 Vandermeersch, B., 1989. ESR dating of the Neanderthal site, Kebara Cave, Israel. J.
914 Archaeol. Sci. 16, 653–659.
915 Schwartz, J., 2016. Beyond *Homo erectus*: Sangiran is key to deciphering the Asian human
916 fossil record and re-evaluating *Homo*. In: Ribot Trafí, F. (Ed.), Homenaje al Dr. José
917 Gibert Clols. Una Vida Dedicada a la Ciencia y al Conocimiento de los Primeros
918 Europeos. Publicaciones Diputación de Granada, Granada, pp. 93-110.
919 Schwartz, J.H., Tattersall, I. 2000. What constitutes *Homo erectus*? Acta Anthropol. Sin.
920 Suppl. 19, 18-22.
921 Schwartz, J.H., Tattersall, I., 2003. The Human Fossil Record, Vol. 2. Craniodental
922 Morphology of Genus *Homo* (Africa and Asia). Wiley-Liss, Hoboken.
923 Sémah, F., Saleki, H., Falguères, C., Féraud, G., Djubiantono, T., 2000. Did Early Man
924 reach Java during the Late Pleistocene? J. Archaeol. Sci. 27, 763–769.
925 Smith, T.M., Olejniczak, A.J., Kupczik, K., Lazzari, V., de Vos, J., Kullmer, O., Schrenk, F.,
926 Hublin, J.-J., Jacob, T., Tafforeau, P., 2009. Taxonomic assessment of the Trinil molars
927 using non-destructive 3D structural and development analysis. PaleoAnthropology 2009,
928 117–129.
929 Smith, T.M., Houssaye, A., Kullmer, O., Le Cabec, A., Olejniczak, A.J., Schrenk, F., de Vos,
930 J., Tafforeau, P., 2018. Disentangling isolated dental remains of Asian Pleistocene
931 hominins and pongines. PloS One 13, e0204737.
932 Spoor, F., 1993. The comparative morphology and phylogeny of the human bony labyrinth.
933 Ph.D. Dissertation, University of Utrecht.
934 Spoor, F., Zonneveld, F., 1994. The bony labyrinth in *Homo erectus*: A preliminary report.
935 Cour. Forsch.-Inst. Senck. 171, 251–256.
936 Spoor, F., Zonneveld., F., 1995. Morphometry of the primate bony labyrinth: a new method
937 based on high-resolution computed tomography. J. Anat. 186, 271–286.

938 Spoor, F., Zonneveld., F., 1998. Comparative review of the human bony labyrinth. Yearb.
939 Phys. Anthropol. 41, 211–251.
940 Spoor, F., Wood, B., Zonneveld, F., 1994. Implications of early hominid labyrinthine
941 morphology for evolution of human bipedal locomotion. Nature 369, 645–648.
942 Spoor, F., Hublin, J.-J., Braun, M., Zonneveld, F., 2003. The bony labyrinth of Neanderthals.
943 J. Hum. Evol. 44, 141–165.
944 Thompson, J.C., Carvalho, S., Marean, C.W., Alemseged, Z., 2019. Origins of the human
945 predatory pattern. The transition to large-animal exploitation by early hominins. Curr.
946 Anthropol. 60, 1–23.
947 Thorne, A., Wolpoff, M., 1982. Regional continuity in Australasian Pleistocene hominid
948 evolution. Am. J. Phys. Anthropol. 55, 337–49.
949 Tyler, D.E., 2001. *Meganthropus*: Cranial fossils from Java. Hum. Evol. 16, 81–101.
950 Tyler, D.E., 2003. Sangiran 5, (‘‘*Pithecanthropus dubius”*), *Homo erectus*, ‘‘*Meganthropus*,*”*
951 or *Pongo*? Hum. Evol. 18, 229–242.
952 Tyler, D.E., 2004. An examination of the taxonomic status of the fragmentary mandible
953 Sangiran 5, (*Pithecanthropus dubius*), *Homo erectus*, ‘‘*Meganthropus”*, or *Pongo*? Quat.
954 Int. 117, 125–130.
955 Tyler, D.E., Sartono, S., 2001. A new *Homo erectus* cranium from Sangiran, Java. Hum.
956 Evol. 16, 13–25.
957 Urciuoli, A., Zanolli, C., Beaudet, A., Dumoncel, J., Santos, F., Moyà-Solà, S., Alba, D.M.,
958 2020. The evolution of the vestibular apparatus in apes and humans. eLife 9, e51261.
959 Urciuoli, A., Zanolli, C., Almécija, S., Beaudet, A., Dumoncel, J., Morimoto, N., Nakatsukasa,
960 M., Moyà-Solà, S., Begun, D.R., Alba, D.M., 2021a. Reassessment of the phylogenetic
961 relationships of the late Miocene apes *Hispanopithecus* and *Rudapithecus* based on
962 vestibular morphology. Proc. Natl. Acad. Sci. USA 118, e2015215118.
963 Urciuoli, A., Zanolli, C., Beaudet, A., Pina, M., Almécija, S., Moyà-Solà, S., Alba, D.M.,
964 2021b. A comparative analysis of the vestibular apparatus in *Epipliopithecus*
965 *vindobonensis*: Phylogenetic implications. J. Hum. Evol. 151, 102930.

Ward, D. L., Pomeroy, E., Schroeder, L., Viola, T. B., Silcox, M.T., Stock, J.T., 2020. Can bony labyrinth dimensions predict biological sex in archaeological samples? J. Archaeol. Sci. Rep. 31, 102354.

Watanabe, N., Kadar, D., 1985.Quaternary Geology of the Hominid Fossil Bearing Formations in Java. Geological Research and Development Centre, Bandung.

Weidenreich, F., 1945. Giant early man from Java and South China. Anthropol. Pap. Am. Mus. Nat. Hist. 40, 1–134.

Weidenreich, F., 1956. Apes, Giants, and Man. University of Chicago Press, Chicago.

Wolpoff, M.H., 1996. Human Evolution. McGraw-Hill, New York.

Wolpoff, M.H., Hawks, J., Frayer, D.W, Huntley, K., 2001. Modern human ancestry at the peripheries: A test of the replacement theory. Science 291, 293–297.

Wood, B., Collard, M., 1999. The changing face of genus *Homo*. Evol. Anthropol. 8, 195–207.

Wu, X.-J., Zhang, Y., 2016. The temporal bony labyrinthine morphology of Lantian *Homo erectus* from Gongwangling, Shaanxi province. Acta Anthropol. Sin. 35, 14–23.

Wu, X.-J., Crevecoeur, I., Liu, W., Xing, S., Trinkaus, E., 2014. Temporal labyrinths of eastern Pleistocene humans. Proc. Natl. Acad. Sci. USA, 111, 10509–10513.

Zanolli, C., Kullmer, O., Kelley, J., Bacon, A.-M., Demeter, F., Dumoncel, J., Fiorenza, L., Grine, F.E., Hublin, J.-J., Nguyen, A.T., Nguyen, T.M.H., Pan, L., Schillinger, B., Schrenk, F., Skinner, M.M., Ji, X., Macchiarelli, R., 2019. Evidence for increased hominid diversity in the Early to Middle Pleistocene of Indonesia. Nat. Ecol. Evol. 3, 755–764.

Zhu, R.X., Potts, R., Pan, Y.X., Yao, H.T., Lü, L.Q., Zhao, X., Gao, X., Chen, L.W., Gao, F., Deng, C.L., 2004. Early evidence of the genus *Homo* in East Asia. J. Hum. Evol. 55, 1075–1085.

Figure captions

Figure 1. Lateral view of Sangiran 2 calvaria (a) and Sangiran 4 partial cranium (b). Not to scale. 3D model renderings of the Sangiran 2 (c, in red) and Sangiran 4 (d, in blue) cochlea in lateral (top) and inferior (bottom) views. Scale bar = 5 mm.

Figure 2. Proportions of the first cochlear turn cross section. a) Bivariate ordinary least square regression between log-transformed cross section height (log Sh) and width (log Sw). b) Box-and-whisker plot of cochlear cross section aspect ratio (Sw/Sh). Horizontal lines correspond to the median, boxes depict interquartile range, whiskers represent maximum and minimum values within 1.5 times the interquartile range, and black dots are outliers. The 3D models at the low and high end of the distribution represent extreme morphologies of cross-sectional shape (shaded in red): round (above) vs. oval (below).

Figure 3. Box-and-whisker plots of the cochlear variables analyzed in the present study and derived from Conde-Valverde et al. (2018): a) number of turns (NT); b) cochlear volume (Vol, in mm^3); c) cochlear length (CL, in mm); d) length of the first cochlear turn (L1, in mm); e) length of the third cochlear turn (L3, in mm); f) size of the first turn radius (R1, in mm); g) size of the third turn radius (R3, in mm); h) cochlear thickness (CTh, in mm); i) height of the cross section of the first cochlear turn (Sh, in mm); j) width of the cross section of the first cochlear turn (Sw, in mm). Horizontal lines correspond to the median, boxes depict interquartile range, whiskers represent maximum and minimum values within 1.5 times the interquartile range, and black dots are outliers.

Figure 4. Box-and-whisker plots of cochlear turn proportions. Vertical lines correspond to the median, boxes depict interquartile range, whiskers represent maximum and minimum values within 1.5 times the interquartile range, and black dots are outliers. The wireframe on the right depicts the three cochlear turns with red (L1), green (L2), and blue (L3) spheres.

Figure 5. Patterns of cochlear shape variation among hominins based on the results of a principal component analysis, as depicted by bivariate plots between the first two principal components: PC2 vs. PC1. The variance explained by each PC is given along the corresponding axis. Four groups (modern humans, australopiths [*Australopithecus* + *Paranthropus*], Neanderthals, and Sima de los Huesos) were defined a priori. The convex hulls corresponding to the range of variation of each group are colored as follows: modern humans = blue; australopiths = brown; Neanderthals = lilac; Sima de los Huesos = green.

Figure 6. Patterns of cochlear shape variation among hominins based on the results of a canonical variates analysis, as depicted by bivariate plots between the first two canonical variates (CV): CV2 vs. CV1. The variance explained by each CV is given along the corresponding axis. Four groups (modern humans, australopiths [*Australopithecus* + *Paranthropus*], Neanderthals, and Sima de los Huesos) were defined a priori, while individual fossil specimens (the *H. erectus* S2 and S4, the early *Homo* SK 27 and SK 847, and the Middle Pleistocene human Aroeira 3) were projected post hoc onto the morphospace. The convex hulls corresponding to the range of variation of each group are colored as follows: modern humans = blue; australopiths = brown; Neanderthals = lilac; Sima de los Huesos = green.

Figure 7. Box-and-whisker plots of the hearing range limit estimates obtained for the studied and comparative samples: a) adjusted high frequency limit (in kHz; at 60db); b) low frequency limit (in Hz; at 60db). Horizontal lines correspond to the median, boxes depict interquartile range, whiskers represent maximum and minimum values within 1.5 times the interquartile range, and black dots are outliers. The plots are presented in logarithmic scale to facilitate the comparison between the results obtained for the high and low frequency limit. Abbreviations: AU = *Australopithecus* + *Paranthropus*; MH = modern humans; NE = Neanderthals; SH = Sima de los Huesos humans

Figure 1_rev

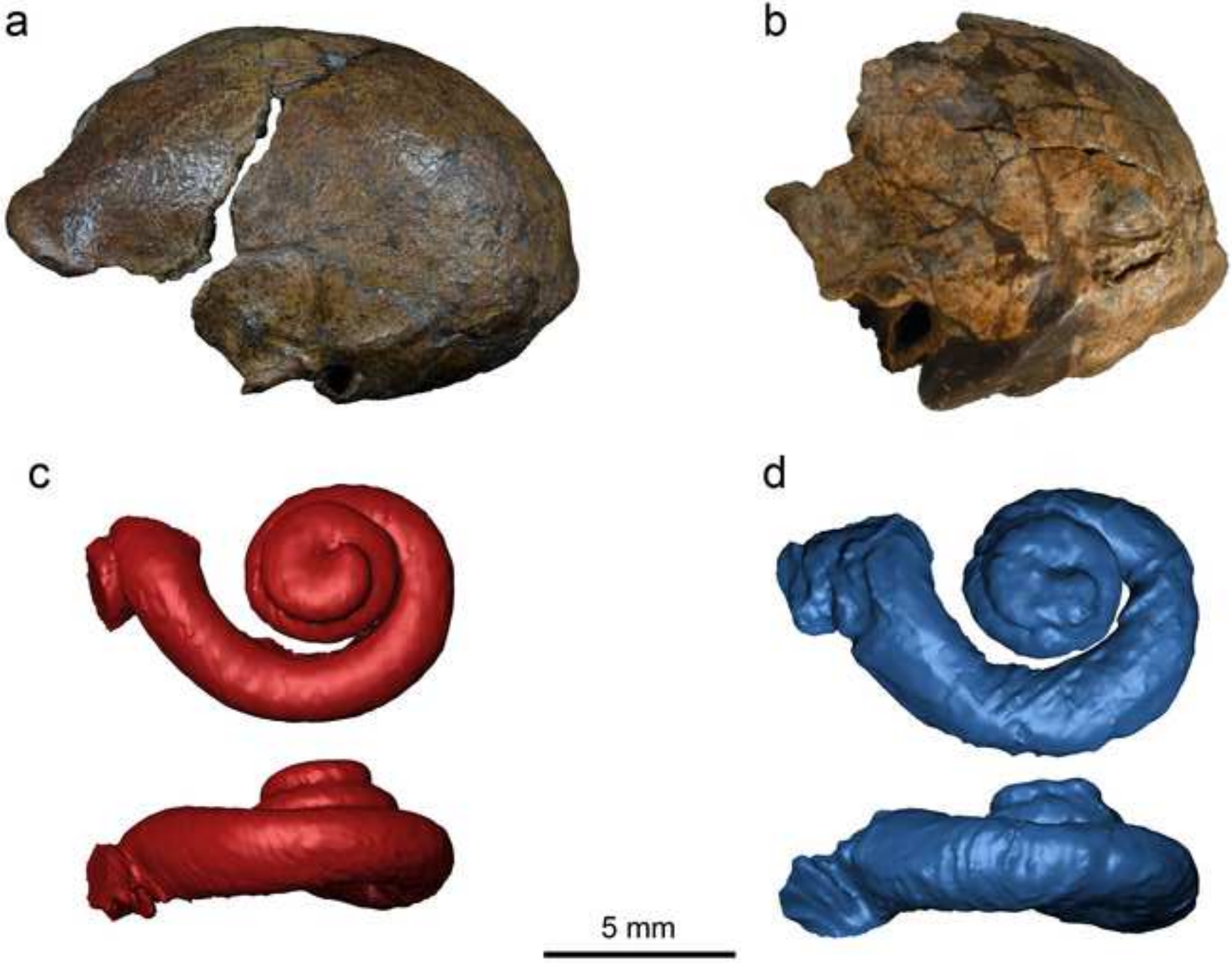

Figure 2

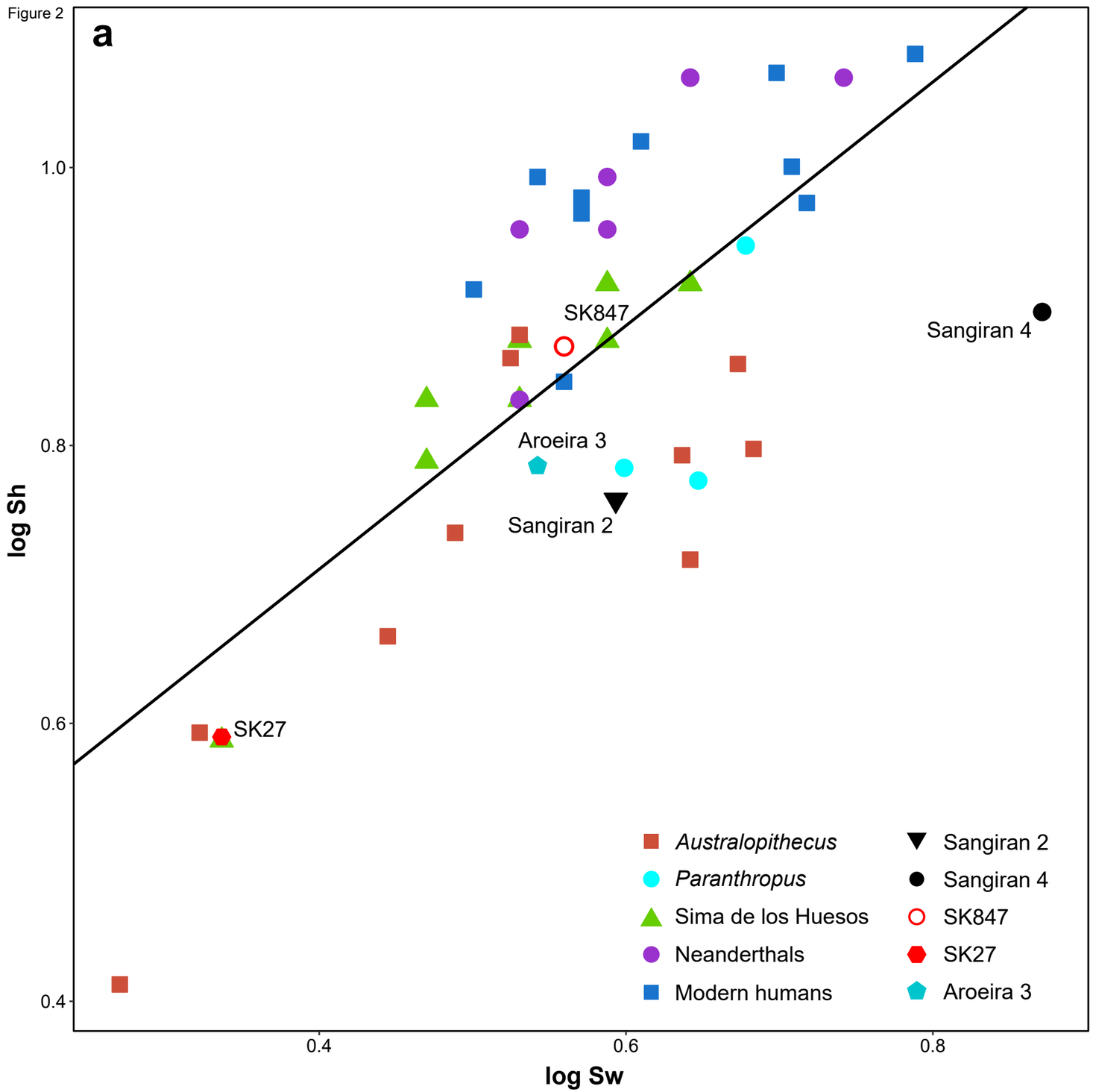
a
1.0
0.8
0.6
0.4
log Sh
0.4
0.6
0.8
log Sw
SK847
Sangiran 4
Aroeira 3
Sangiran 2
SK27
Australopithecus
Paranthropus
Sima de los Huesos
Neanderthals
Modern humans
Sangiran 2
Sangiran 4
SK847
SK27
Aroeira 3

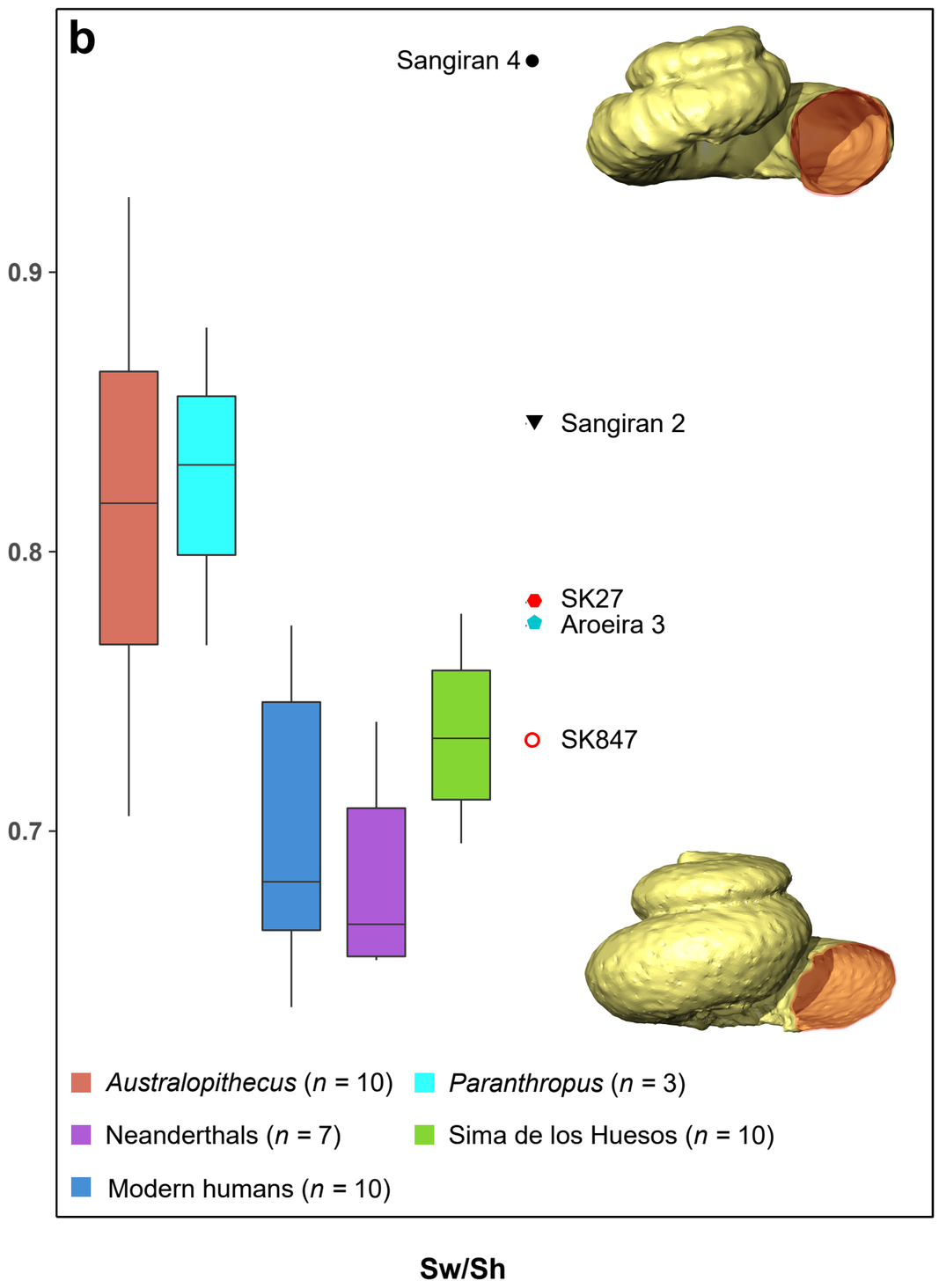
b
Sangiran 4
0.9
0.8
0.7
Sangiran 2
SK27
Aroeira 3
SK847
Australopithecus (n = 10)
Paranthropus (n = 3)
Neanderthals (n = 7)
Sima de los Huesos (n = 10)
Modern humans (n = 10)
Sw/Sh

Figure 3_rev

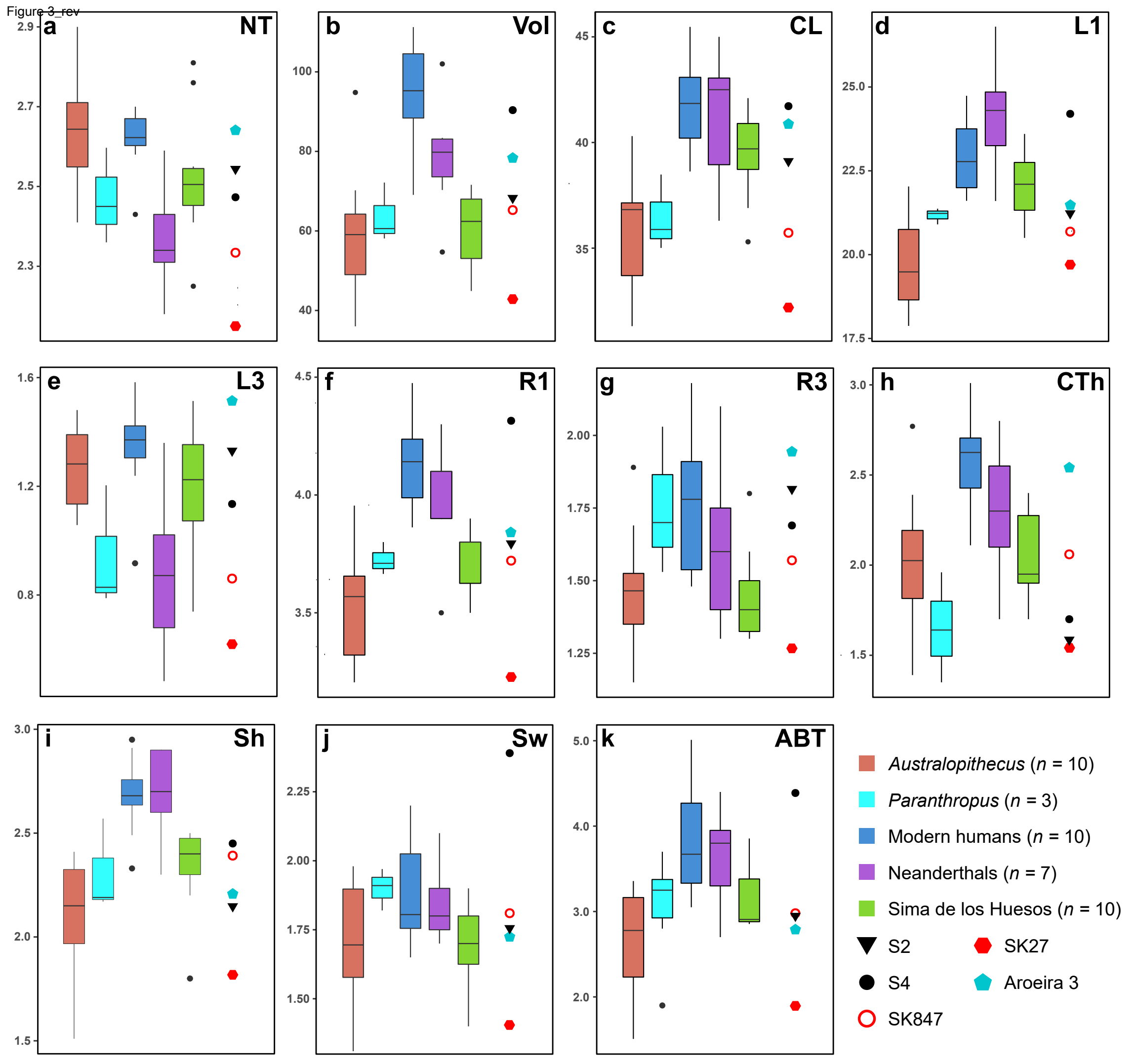
a
NT
2.9
2.7
2.5
2.3
b
Vol
100
80
60
40
c
CL
45
40
35
d
L1
25.0
22.5
20.0
17.5
e
L3
1.6
1.2
0.8
f
R1
4.5
4.0
3.5
g
R3
2.00
1.75
1.50
1.25
h
CTh
3.0
2.5
2.0
1.5
i
Sh
3.0
2.5
2.0
1.5
j
Sw
2.25
2.00
1.75
1.50
k
ABT
5.0
4.0
3.0
2.0
Australopithecus (n = 10)
Paranthropus (n = 3)
Modern humans (n = 10)
Neanderthals (n = 7)
Sima de los Huesos (n = 10)
S2
SK27
S4
Aroeira 3
SK847

Figure 4_rev

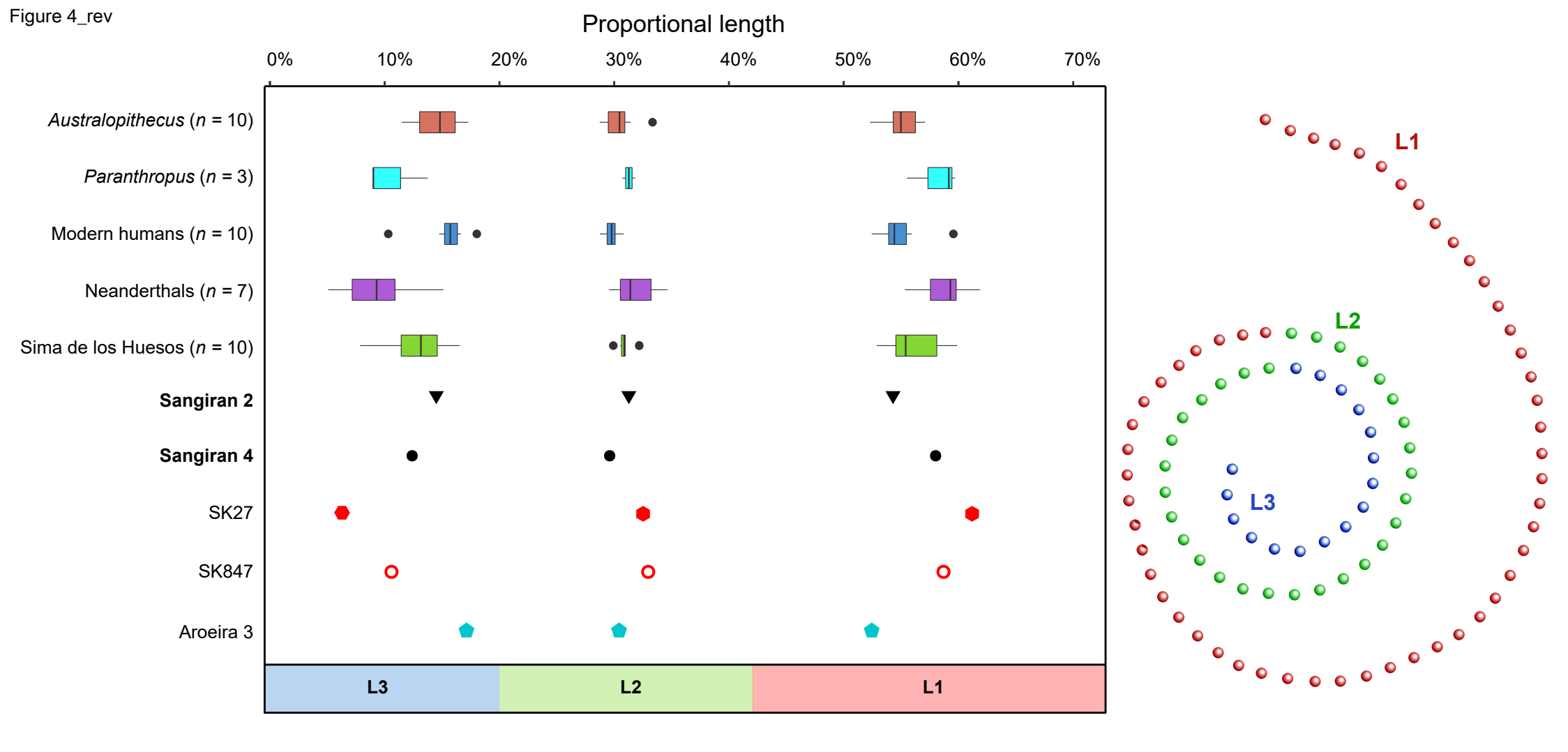
Proportional length
0%
10%
20%
30%
40%
50%
60%
70%
Australopithecus (n = 10)
Paranthropus (n = 3)
Modern humans (n = 10)
Neanderthals (n = 7)
Sima de los Huesos (n = 10)
Sangiran 2
Sangiran 4
SK27
SK847
Aroeira 3
L3
L2
L1
L1
L2
L3

Figure 5_rev

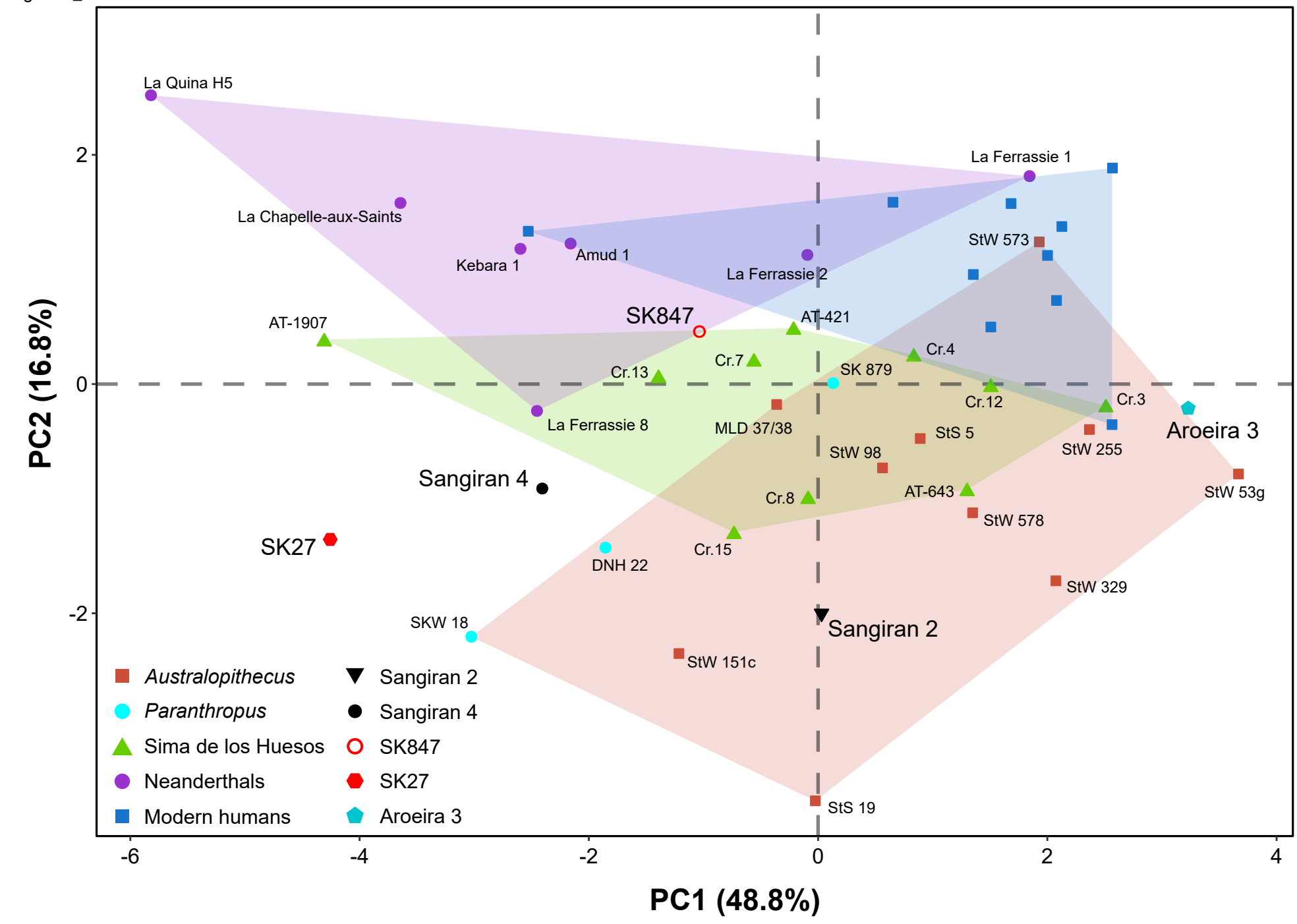
La Quina H5
La Chapelle-aux-Saints
Kebara 1
Amud 1
La Ferrassie 1
La Ferrassie 2
StW 573
AT-1907
SK847
AT-421
Cr.7
Cr.13
Cr.4
SK 879
Cr.12
Cr.3
La Ferrassie 8
MLD 37/38
StS 5
StW 255
Aroeira 3
StW 98
Sangiran 4
Cr.8
AT-643
StW 53g
StW 578
SK27
Cr.15
DNH 22
StW 329
SKW 18
Sangiran 2
StW 151c
StS 19
Australopithecus
Paranthropus
Sima de los Huesos
Neanderthals
Modern humans
Sangiran 2
Sangiran 4
SK847
SK27
Aroeira 3
PC2 (16.8%)
PC1 (48.8%)
2
0
-2
-6
-4
-2
0
2
4

Figure 6_rev

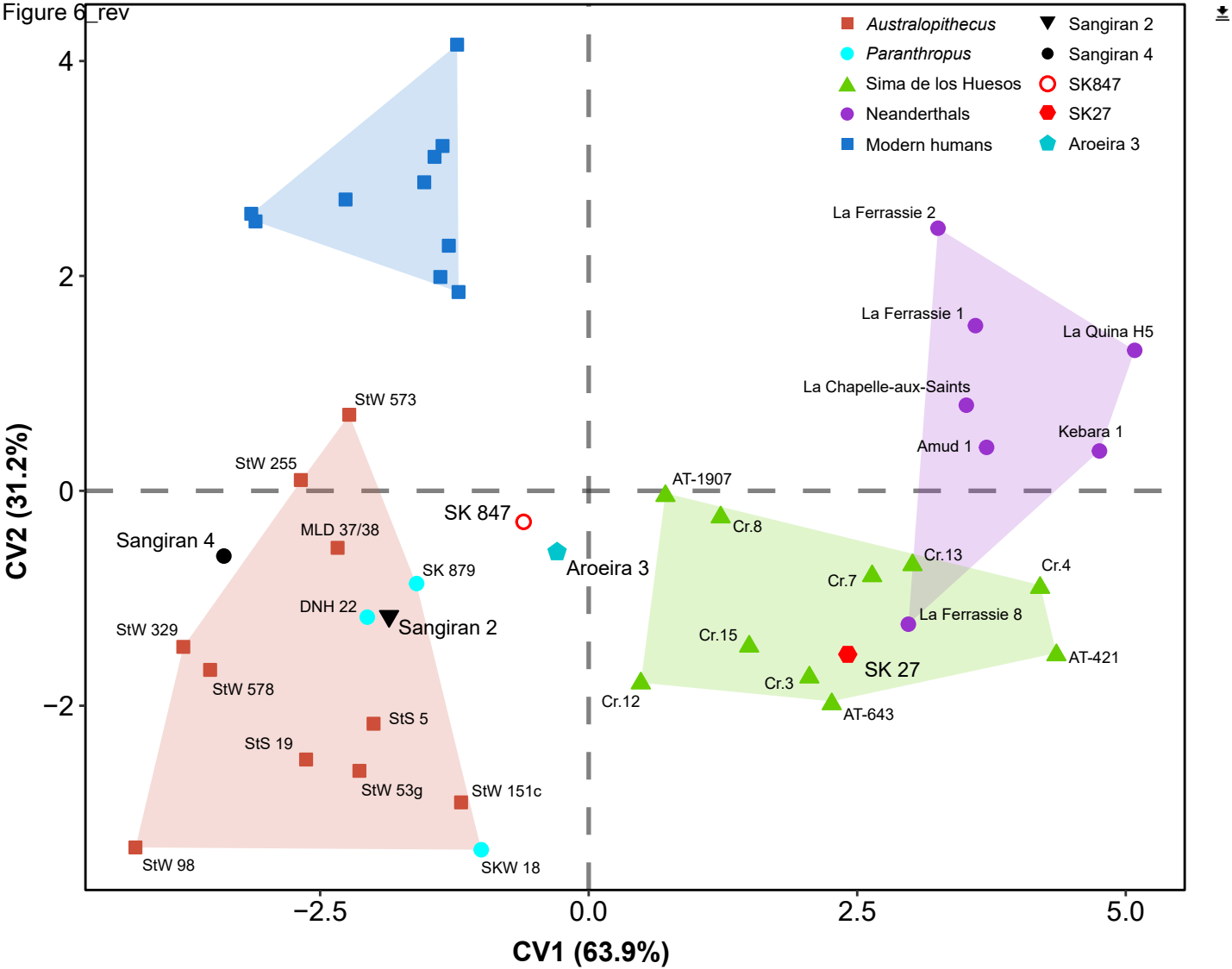
Australopithecus
Paranthropus
Sima de los Huesos
Neanderthals
Modern humans
Sangiran 2
Sangiran 4
SK847
SK27
Aroeira 3
La Ferrassie 2
La Ferrassie 1
La Quina H5
La Chapelle-aux-Saints
Kebara 1
Amud 1
AT-1907
Cr.8
Cr.13
Cr.4
Cr.7
La Ferrassie 8
Cr.15
SK 27
AT-421
Cr.3
Cr.12
AT-643
StW 573
StW 255
Sangiran 4
MLD 37/38
SK 847
SK 879
Aroeira 3
DNH 22
Sangiran 2
StW 329
StW 578
StS 5
StS 19
StW 53g
StW 151c
StW 98
SKW 18
4
2
0
−2
−2.5
0.0
2.5
5.0
CV2 (31.2%)
CV1 (63.9%)

Figure_7_R2

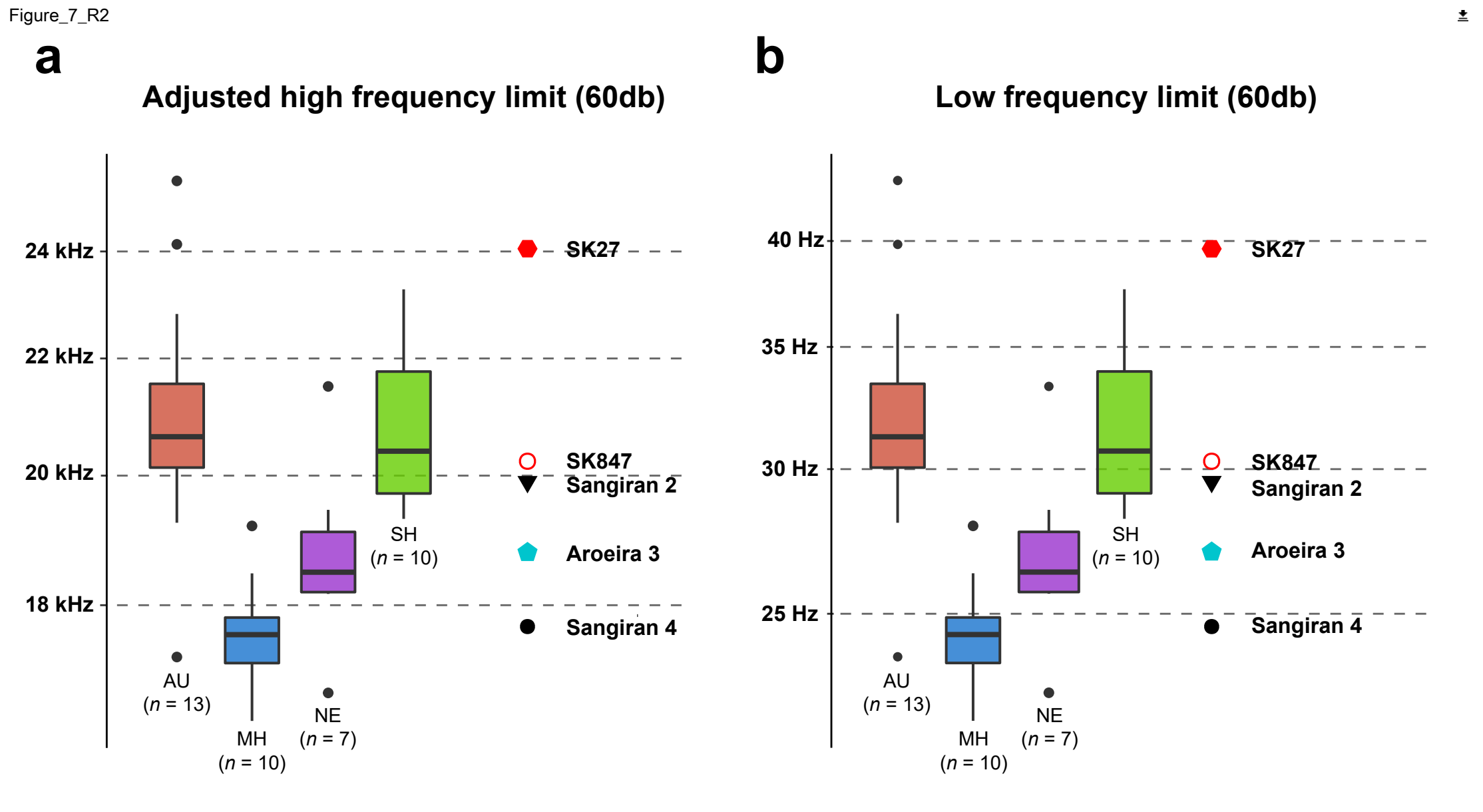
a
Adjusted high frequency limit (60db)
24 kHz
22 kHz
20 kHz
18 kHz
AU
(n = 13)
MH
(n = 10)
NE
(n = 7)
SH
(n = 10)
SK27
SK847
Sangiran 2
Aroeira 3
Sangiran 4
b
Low frequency limit (60db)
40 Hz
35 Hz
30 Hz
25 Hz
AU
(n = 13)
MH
(n = 10)
NE
(n = 7)
SH
(n = 10)
SK27
SK847
Sangiran 2
Aroeira 3
Sangiran 4

Table 1

Cochlear variables measured for Indonesian *Homo erectus* (Sangiran 2 and 4) and the comparative sample.

Specimens/samples	CL	L1	L3	Vol	Sw	Sh	R1	R3	CTh	NT	ABT
Indonesian *H. erectus*											
Sangiran 2	39.04	21.20	5.66	66.80	1.81	2.14	3.79	1.81	1.58	2.54	2.93
Sangiran 4	41.72	24.20	5.17	89.13	2.39	2.45	4.32	1.57	1.70	2.47	4.39
Early *Homo*:											
SK27	32.11	19.65	2.02	41.34	1.4	1.81	3.2225	1.26	1.54	2.15	1.9
SK847	35.73	20.70	3.52	63.74	1.75	2.39	3.7225	1.69	2.06	2.333	2.99
Middle Pleistocene *Homo*											
Aroeira 3	40.94	21.47	7.01	76.46	1.72	2.20	3.84	1.94	2.54	2.64	2.80
Australopithecus (*n* = 10)											
Mean (SD)	35.86 (2.62)	19.70 (1.27)	5.23 (0.85)	58.97 (15.75)	1.70 (0.22)	2.10 (0.27)	3.53 (0.23)	1.46 (0.21)	2.01 (0.39)	2.63 (0.15)	2.63 (0.63)
Range	31.31–40.30	17.88–22.03	3.59–6.36	36.02–94.82	1.31–1.98	1.51–2.41	3.21–3.96	1.15–1.89	1.39–2.77	2.41–2.90	1.51-3.57
Paranthropus (*n* = 3)											
Mean (SD)	36.46 (1.48)	21.17 (0.20)	3.89 (0.99)	63.62 (6.13)	1.90 (0.06)	2.31 (0.18)	3.73 (0.13)	1.75 (0.06)	1.65 (0.25)	2.47 (0.10)	3.21 (0.46)
Range	35.01–38.48	20.90–21.37	3.16–5.30	58.11–72.17	1.82–1.97	2.17–2.57	3.67–3.80	1.53–2.03	1.35–1.96	2.36–2.60	2.85-3.86
Neanderthals (*n* = 7)[a]											
Mean (SD)	41.11 (2.89)	24.13 (1.53)	3.90 (1.57)	78.56 (13.27)	1.84 (0.13)	2.70 (0.21)	3.99 (0.24)	1.61 (0.26)	2.30 (0.35)	2.37 (0.13)	3.63 (0.53)
Range	36.30–45.00	21.60–26.80	2.00–6.80	54.70–102.00	1.70–2.10	2.30–2.90	3.50–4.30	1.30–2.10	1.70–2.80	2.18–2.59	2.70-4.40

Sima de los Huesos (*n* = 10)[a]											
Mean (SD)	39.41 (1.96)	22.1 (0.95)	5.10 (1.06)	60.31 (8.85)	1.71 (0.15)	2.33 (0.20)	3.73 (0.12)	1.45 (0.15)	2.03 (0.24)	2.53 (0.15)	3.11 (0.49)
Range	35.30–42.10	20.50–23.60	2.90–6.60	44.90–71.60	1.40–1.90	1.80–2.50	3.50–4.30	1.30–2.10	1.70–2.80	2.18–2.59	1.90-3.70
Modern humans (*n* = 10)											
Mean (SD)	41.81 (2.01)	22.91 (1.06)	6.46 (0.94)	91.01 (9.65)	1.88 (0.17)	2.68 (0.17)	4.13 (0.18)	1.75 (0.22)	2.59 (0.26)	2.62 (0.08)	3.81 (0.61)
Range	38.62–45.47	21.61–24.74	4.12–7.61	72.64–107.98	1.65–2.20	2.33–2.95	3.86–4.48	1.48–2.18	2.11–3.01	2.43–2.7	3.05-5.01

Abbreviations: CL = cochlear length (mm); L1 = length of the first turn (mm); L3 = length of the third turn (mm); Vol = cochlear volume (mm^3); Sw = width of the first turn cross section (mm); Sh = height of the first turn cross section (mm); R1 = radius of the 1st (basal) turn (mm); R3 = radius of the 3rd (apical) turn (mm); CTh = cochlear thickness (mm); NT = number of turns; ABT = cross-sectional area at the first basal turn.

[a] Data taken from Conde-Valverde et al. (2019).

Table 2

Z-scores computed for individual fossil specimens based on the distribution (mean and SD) of Sw/Sh in the various groups included in the comparative sample[a].

Fossil specimens	AU	NE	SH	MH
Sangiran 2	0.46	**4.56**	**4.11**	**3.01**
Sangiran 4	**2.43**	**8.20**	**8.91**	**5.70**
SK27	-0.64	**2.52**	1.44	1.50
SK847	-1.26	1.36	-0.09	0.65
Aroeira 3	-0.51	**2.76**	1.75	1.68

Abbreviations: AU = Australopiths (*Australopithecus* + *Paranthropus*); NE = Neanderthals; SH = Sima de los Huesos; MH = modern humans; Sw/Sh = ratio between the width and height of the cochlear first turn cross section.

[a] Z-scores greater than |1.96|, indicating significant differences relative to the reference distributions, are bolded.

Table 3

Shape variable loadings for the first two principal components (PCs) of the principal components analysis depicted in Figure 5.

Variable	PC1	PC2
NT*	0.0500	-0.5959
CL*	-0.3196	-0.0835
L1*	-0.4151	-0.0073
L3*	0.4265	-0.0667
Sw*	-0.3192	-0.0588
Sh*	-0.2754	0.5068
$Vol^{1/3}$*	-0.3921	0.0156
R1*	-0.4217	-0.1172
R3*	-0.0414	-0.2095
CTh*	0.1734	0.5615

Abbreviations: NT* = number of turns; CL* = cochlear length; L1* = length of the first turn; L3* = length of the third turn; Sw* = width of the first turn cross section; Sh* = height of the first turn cross section; $Vol^{1/3}$* = cube root of cochlear volume; R1* = radius of the first turn; R3* = radius of the third turn; CTh* = cochlear thickness.

Table 4

Classification results of a canonical variate analysis based on cochlear variables and performed using the four groups distinguished among the comparative sample. For each group distinguished a priori, the number of individuals classified in each group and the percentage of correctly classified individuals is provided. Cross-validated results are given within parentheses.

Group	%	*n*			
		AU	MH	NE	SH
Australopiths	92.3% (84.6%)	12 (11)	1 (2)	0 (0)	0 (0)
MH	100% (100%)	0 (0)	10 (10)	0 (0)	0 (0)
NE	100% (71.4%)	0 (0)	0 (0)	7 (5)	0 (2)
SH	100% (70.0%)	0 (1)	0 (0)	0 (2)	10 (7)

Abbreviations: AU = Australopiths (*Australopithecus* + *Paranthropus*); MH = modern humans; NE = Neanderthals; SH = Sima de los Huesos.

Table 5

Shape variable loadings for the first two canonical variates (CVs) of the canonical variate analysis depicted in Figure 6.

Variable	CV1	CV2
NT*	-8.316	-19.446
CL*	6.078	-5.542
L1*	-0.562	7.637
L3*	-8.699	12.260
Sw*	-18.854	-23.407
Sh*	11.286	16.110
$Vol^{1/3}$*	-30.097	30.358
R1*	-24.654	11.975
R3*	-4.467	7.143
CTh*	-0.069	6.393

Abbreviations: NT* = number of turns; CL* = cochlear length; L1* = length of the first turn; L3* = length of the third turn; Sw* = width of the first turn cross section; Sh* = height of the first turn cross section; $Vol^{1/3}$* = cube root of cochlear volume; R1* = radius of the first turn; R3* = radius of the third turn; CTh* = cochlear thickness.

Table 6

Cross-validated classification results for individual fossil specimens based on a canonical variate analysis of cochlear variables performed using four groups distinguished a priori among the comparative sample.

Fossil specimens	AU	MH	NE	SH
Posterior probabilities[a]				
Sangiran 2	**99.5%**	0.3%	0.0%	0.2%
Sangiran 4	**96.3%**	3.7%	0.0%	0.1%
SK27	0.0%	0.0%	**92.0%**	8.0%
SK847	**95.5%**	2.7%	0.0%	1.8%
Aroeira 3	15.7%	1.5%	0.2%	**82.8%**
Typicality probabilities[b]				
Sangiran 2	**0.141**	0.001	<0.001	0.001
Sangiran 4	<0.001	<0.001	<0.001	<0.001
SK27	<0.001	<0.001	0.001	0.001
SK847	**0.107**	0.004	<0.001	0.003
Aroeira 3	0.012	0.001	<0.001	**0.054**

Abbreviations: AU = Australopiths (*Australopithecus* + *Paranthropus*); MH = modern humans; NE = Neanderthals; SH = Sima de los Huesos.

[a] These probabilities assume that each fossil specimen belongs to one of the four groups defined a priori, so that the sum of probabilities equals 100%. The highest nonsignificant probability (if any) is bolded.

[b] These probabilities denote the probability of having the score of each fossil specimen given membership in a particular group, not the likelihood of group membership in each of the a priori defined groups given a particular score. $p < 0.05$ thus denotes outliers to the distribution of each a priori group. The highest probability for each fossil specimen is bolded.

Table 7

Inferred high and low frequency limits based on cochlear parameters (Kirk and Gosselin-Ildari, 2009).

Specimens/samples	HFL	AHFL	LFL
Indonesian *Homo erectus*			
Sangiran 2	23.45	19.85	29.42
Sangiran 4	20.89	17.69	24.60
Early *Homo*			
SK27	28.41	24.05	39.61
SK847	23.89	20.23	30.29
Middle Pleistocene *Homo*			
Aroeira 3	22.21	18.81	27.06
Australopithecus (*n* = 10)			
Mean (SD)	25.13 (2.64)	21.28 (2.24)	32.91 (5.37)
Range	20.38–30.02	17.26–25.42	23.68–43.15
Paranthropus (*n* = 3)			
Mean (SD)	23.97(0.89)	20.29 (0.75)	30.46 (1.74)
Range	22.73–24.79	19.25–20.99	28.04–32.07
Neanderthals (*n* = 7)			
Mean (SD)	22.16 (1.59)	18.77 (1.35)	27.02 (3.04)
Range	19.80–25.40	16.76–21.50	22.63–33.30
Sima de los Huesos (*n* = 10)			
Mean (SD)	24.58 (1.53)	20.82 (1.29)	31.71 (3.07)
Range	22.81–27.49	19.31–23.27	28.18–37.64
Modern humans (*n* = 10)			
Mean (SD)	20.79 (0.91)	17.60 (0.77)	24.43 (1.66)
Range	19.35–22.67	16.38–19.20	21.84–27.93

Abbreviations: HFL = high frequency limit (kHz) at 60 dB; AHFL = adjusted high frequency limit (kHz) at 60 dB; LFL = low frequency limit (Hz) at 60 dB.

Table 8

Z-scores computed for individual fossil specimens based on the distribution (mean and SD) of AHFL and LFL in the various groups included in the comparative sample.

Fossil specimens	AU	NE	SH	MH
AHFL Z-scores:				
Sangiran 2	-0.59	0.81	-0.74	2.93
Sangiran 4	-1.65	-0.80	-2.42	0.12
SK27	1.47	3.92	2.51	8.40
SK847	-0.40	1.09	-0.45	3.42
Aroeira 3	-1.10	0.03	-1.56	1.57
LFL Z-scores:				
Sangiran 2	-0.60	0.79	-0.75	3.00
Sangiran 4	-1.58	-0.79	-2.31	0.11
SK27	1.49	4.14	2.57	9.14
SK847	-0.42	1.07	-0.46	3.53
Aroeira 3	-1.08	0.01	-1.51	1.58

Abbreviations: AHFL = Adjusted high frequency limit (kHz) at 60 dB; LFL = low frequency limit (kHz) at 60 dB; AU = Australopiths (*Australopithecus* + *Paranthropus*); NE = Neanderthals; SH = Sima de los Huesos; MH = modern humans

Table 9

Updated character state summary combining the information provided in the present study with previously published data[a].

Taxon	CL	%L1	%L3	NT	ABT	Sw/Sh	Vol	CTh
Pan troglodytes	Long	Short	Long	High	Small	Round	Small	Low
Australopiths	Short	**Short**	**Long**	Low	**Small**	**Round**	**Small**	**Low**
Early *Homo*	Short	**Long**	**Short**	**Low/Very low**	**Small**	**Oval-shaped**	**Small**	**Low**
Homo erectus	**Long**	**Intermediate/Long**	**Intermediate/Short**	**Low**	**Small/Large**	**Round**	**Intermedia te/Large**	**Low**
Sima de los Huesos Hominins	Long	Short	Short	Low	Small	**Oval-shaped**	Small	Low
Neanderthals	Long	Long	Very short	Very low	Large	Oval-shaped	Large	High
Modern humans	Long	Long	Short	Low	Large	Oval-shaped	Large	High

Abbreviations: CL = cochlear length; L1% = proportional length of the first turn; %L3 = proportional length of the third turn; NT = number of turns; ABT = cross-sectional area at the first basal turn; Sw/Sh = ratio between the cochlear first turn cross section width; Vol = cochlear volume; CTh = cochlear thickness.

[a] States reported here for the first time or modified relative to Conde-Valverde et al. (2019) are in bold.